BLOCK ERROR RATE OF OPTICAL WIRELESS COMMUNICATION SYSTEMS OVER ATMOSPHERIC TURBULENCE CHANNELS

by

QIAN ZHANG

B.Eng., Tianjin University of Science and Technology, P. R. China, 2010

A THESIS SUBMITTED IN PARTIAL FULFILLMENT OF
THE REQUIREMENTS FOR THE DEGREE OF

MASTER OF APPLIED SCIENCE

in

THE COLLEGE OF GRADUATE STUDIES

(Electrical Engineering)

THE UNIVERSITY OF BRITISH COLUMBIA

(Okanagan)

April 2013

Abstract

Optical wireless communication (OWC) is an innovative and promising technology introduced in recent decades, and it can be used for both indoor and outdoor applications. Outdoor OWC is also an attractive solution to the access network bottle-neck. However, challenges can arise for OWC links with increased atmospheric turbulence levels due to time-varing temperatures and pressures, resulting fading or scintillation. This thesis studies and analyzes the block error rate performance of subcarrier intensity modulation based OWC systems employing both noncoherent and coherent binary modulations over various atmospheric turbulence channels. The block error rate is a meaningful performance metric in the slow fading turbulence channels because the fading coefficients are constant over the duration of a block of bits. For the Gamma-Gamma turbulence channels, we obtain highly accurate block error rate expressions in terms of an infinite series for noncoherent binary modulations. With coherent binary phase shift keying, we first propose a new sum of exponentials approximation of the Gaussian Q-function, and then develop the corresponding block error rate expression. For the lognormal turbulence channels, we use the Gauss-Laguerre quadrature method to obtain an accurate estimation of the block error rate.

Table of Contents

List of Figures

List of Acronyms

Acronyms	Definitions
4G	Fourth Generation
AWGN	Additive White Gaussian Noise
BER	Bit Error Rate
BLER	Block Error Rate
BPSK	Binary Phase Shift Keying
DPSK	Differential Phase Shift Keying
FSO	Free-space Optical
Gbit/s	Gigabit per Second
IM/DD	Intensity Modulation and Direct Detection
LANs	Local Area Networks
MANs	Metropolitan Area Networks
MPSK	M-ary Phase Shift Keying
NCFSK	Noncoherent Frequency Shift Keying
NRZ	Non-Return-to-Zero
OOK	On-Off Keying
OWC	Optical Wireless Communication
PDF	Probability Density Function
PPM	Pulse Position Modulation
RF	Radio Frequency
RV	Random Variable

RZ	Return-to-Zero
SNR	Signal-to-Noise Ratio
SIM	Subcarrier Intensity Modulation
WANs	Wide Area Networks

Acknowledgments

I am deeply grateful to my supervisor Prof. Julian Cheng for his enthusiasm, guidance, advice, encouragement, and support. He granted me great flexibility and freedom in my research work. He taught me academic knowledge and research skills. I will continue to be influenced by his rigorous scholarship, clarity in thinking, and professional integrity. It is my honor to study and research under his supervision.

I would like to express my thanks to Prof. Yang Cao for his willingness to serve as my external examiner. I would also like to thank Prof. Stephen O'Leary and Prof. Jahangir Hossain for serving on the committee. I really appreciate their valuable time and constructive comments on my thesis.

I owe many people for their generosity and support during my MASc study at The University of British Columbia. I would like to thank my dear colleagues Luanxia Yang, Xuegui Song, Mingbo Niu, Nianxin Tang, Md. Zoheb Hassan, and Fan Yang for sharing their academic experiences and constructive viewpoints generously with me during our discussions. I would also like to thank my dear friends Haibo Feng, Wendi Zhang, Yipin Guo, and Jia Xu for sharing my excitement and encouraging me when I was in frustration during this journey. I would also like to thank all my friends in Tianjin and Beijing.

Finally, I would like to thank my parents for their patience, understanding, and support all these years. All my achievements would not have been possible without their constant encouragement and support.

Chapter 1

Introduction to OWC

1.1 Background and Motivation

Optical wireless communication (OWC) is a technology that uses light to transmit information bits through a free-space channel between two points. The first optical wireless communication experiment over an unguided channel was performed by Alexander Graham Bell in 1880, and this invention was called photophone [1]. Although the photophone was an important invention, it was influenced by the ambient light sources in the course of light transmission. The fortune of OWC changed in the 1960s with the introduction of the semiconductor laser, which is the most important discovery of optical sources. Around 1970, Nippon Electric Company (NEC) built the first laser link to handle commercial traffic in Japan. Since then, OWC has been an active research area. This technology was also applied to deep space applications by National Aeronautics and Space Administration (NASA) and European Space Agency (ESA) with programmes such as the Mars Laser Communication Demonstration (MLCD) and the Semiconductor-laser Inter-satellite Link Experiment (SILEX). With the development and maturity of optoelectronic devices, OWC has again drawn recent research interests. In the last few years, several successful field trials have further encouraged renewed investigations within the OWC research community. These activities have led to broader scale of commercialization and wider deployment of OWC equipment infrastructures.

In recent years, OWC is becoming an alternative technology to optical fiber and radio frequency (RF) communications. OWC technology is also a viable solution to the 'last mile' bottleneck problem, providing a license-free high data rate service. The OWC infrastructures

are relatively low cost and have much lower deployment cost than that of fibre optic networks. The outdoor OWC, also known as free-space optical (FSO) communication, can be divided into long-range free space links and short-range links [2]. The long-range free space links are mainly used in the area of intersatellite links. The short-range links are typically used as the first or last mile access by taking broadband services to home or providing backhaul solution. These links are also used as a high bandwidth bridge between the local area networks (LANs), metropolitan area networks (MANs), and wide area network (WANs).

In spite of a number of advantages of OWC systems, challenges remain to fully exploit the potentials of OWC technology. One main challenge encountered in OWC is the atmospheric attenuation caused by absorption, scattering and fluctuation of the optical signals. Eye safety, wavelengths noise, fog, rain and snow can also be concerns. Another important challenge is the atmospheric scintillation, which is caused by atmospheric turbulence. The atmospheric turbulence is a random effect that is considered as the most serious effect on propagating laser beams through the atmospheric channels. In OWC, the turbulence fading channel is typically slow; therefore, we propose to use the block error rate (BLER) to evaluate the error rate performance of OWC systems. In this thesis, we will focus on analysing the BLER performance on various digital modulations operating on several commonly used atmospheric turbulence channels.

1.2 Literature Review

OWC has great potentials for applications in fourth-generation (4G) wireless systems and can be a key building block for future wide-area wireless data networks [3], [4]. Such networks are being deployed and will include several complementary access technologies with high channel capacities, multiple transceivers, and gigabit per second (Gbit/s) data rates [4].

Fig. 1.1 shows the block diagram of an optical communication system through the atmosphere. The information generated by a source is modulated into an electrical waveform by an electrical modulator. In the optical modulator, the intensity of a light source is modulated

by the output signal of the electrical modulator. A laser diode generates optical signals, and a telescope is typically used at the transmitter to determine the direction and size of the laser beam. The receiver includes an optical front end, a photodetector, and a demodulator. The optical front end has lenses which are used to focus the received optical field onto a photodetector. The photodetector converts the received optical field to an electrical signal, which is then demodulated. The demodulated bits are fed into an information sink.

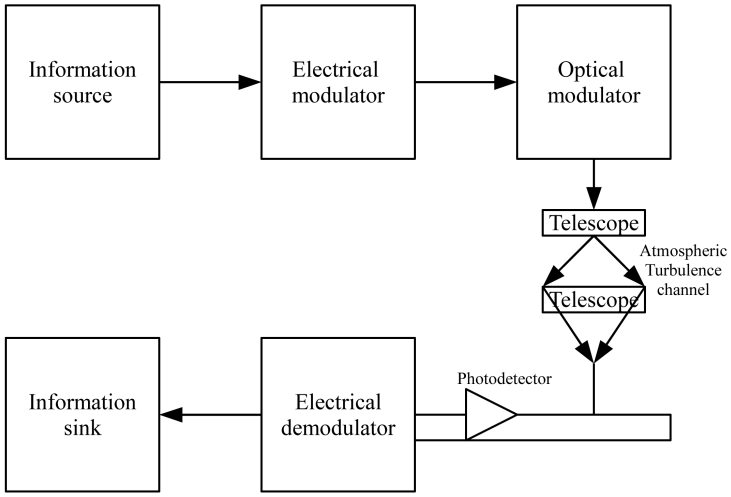

Figure 1.1: Block diagram of an optical communication system through atmospheric turbulence channels.

On-off keying (OOK) is the most widely used signal modulation for OWC systems with direct detection (IM/DD) due to its simplicity in design and low cost [5], [6]. In atmospheric turbulence, however, an OOK based system requires time-varying adaptive detection thresholds. Such systems are also subject to channel estimation errors. In practice, for simplicity, OOK based systems are often implemented with a predetermined fixed detection threshold [7]. In the presence of atmospheric turbulence, the bit error rate (BER) of OOK modulation is determined by both the turbulence level and the fixed detection threshold, and it cannot be made arbitrarily small by increasing signal-to-noise ratio (SNR) [7]. To overcome the drawbacks of OOK optical modulations, PPM has been proposed as an alternative to the OOK modula-

tion. The performance of pulse position modulation (PPM) has been extensively studied in atmospheric turbulence channels in [8], [9], [10]. The PPM improves the power efficiency compared to the OOK. However, the PPM modulation needs a complex transceiver design because of the tight synchronization technique, and it also has a higher bandwidth requirement than the OOK modulation technique. Another attractive modulation technique is subcarrier intensity modulation (SIM), which was first proposed for OWC systems in [11]. The authors studied the error rate performance for differential phase shift keying (DPSK) and M-ary phase shift keying (MPSK) modulations over lognormal turbulence channels both theoretically and experimentally. The error rate performance of SIM based OWC systems for various modulations over different atmospheric turbulence channels was studied in [7], [12], [13], [14].

An optical wave typically experiences irradiance fluctuations when it is propagated through the atmosphere. This phenomenon is referred to as the optical scintillation or turbulent-induced fading. The optical scintillation is caused by the random fluctuations of refractive index due to the temperature and pressure variations along the optical signal propagation. In weak turbulence regimes, the resulting irradiance fluctuations can be characterized by the Rytov variance, which is defined for a plane wave or a spherical wave, respectively, as [15], [16]

$$\sigma_p^2 = 1.23 C_n^2 k^{7/6} L^{11/6} \tag{1.1}$$

and

$$\sigma_l^2 = 0.5 C_n^2 k^{7/6} L^{11/6} \tag{1.2}$$

where L is the link distance, $k = 2\pi/\lambda$, λ is the wavelength, and C_n^2 denotes the index of refraction structure parameter and varies form $10^{-13} m^{-2/3}$ for strong turbulence to $10^{-17} m^{-2/3}$ for weak turbulence. Under the assumption of plane wave propagation, we define the weak turbulence channel when the Rytov variance is much less than unity ($\sigma_p^2 < 0.3$), while the strong turbulence channel or the saturation regime is corresponding to the Rytov variance much

greater than unity ($\sigma_p^2 \gg 1$). Moderate turbulence channel is defined as $\sigma_p^2 \approx 1$ [17].

The scintillation index is another important parameter related to the atmospheric turbulence level, and it is defined as the normalized variance of irradiance fluctuations

$$\sigma_I^2 = \frac{Var[I]}{(E[I])^2} = \frac{E[I^2] - (E[I])^2}{(E[I])^2} = \frac{E[I^2]}{(E[I])^2} - 1 \tag{1.3}$$

where I is the optical irradiance, and $E[\cdot]$ is the expectation operation. The scintillation index for a plane wave and that for a spherical wave with negligible inner scale are related to the Rytov variance through [18]

$$(\sigma_I^2)_{plane} = \exp\left(\frac{0.54\sigma_p^2}{\left(1+1.22\sigma_p^{\frac{12}{5}}\right)^{\frac{7}{6}}} + \frac{0.509\sigma_p^2}{\left(1+0.69\sigma_p^{\frac{12}{5}}\right)^{\frac{5}{6}}}\right) - 1 \tag{1.4}$$

and

$$(\sigma_I^2)_{sphere} = \exp\left(\frac{0.17\sigma_l^2}{\left(1+0.167\sigma_l^{\frac{12}{5}}\right)^{\frac{7}{6}}} + \frac{0.225\sigma_l^2}{\left(1+0.259\sigma_l^{\frac{12}{5}}\right)^{\frac{5}{6}}}\right) - 1. \tag{1.5}$$

In order to evaluate the performance of OWC systems, several statistical models have been proposed to describe the irradiance fluctuation. The lognormal turbulence model has been studied in [19], [20], [21]. The lognormal distribution is one of the most widely used turbulence models, but it is only applicable for weak turbulence conditions. The Gamma-Gamma distribution has recently emerged as a useful turbulence model because it provides a good fit to the experimental measurements of irradiance for both weak and strong turbulence channels [16]. The Gamma-Gamma turbulence model also has the K-distributed model and negative exponential model as the special cases. The K-distribution is commonly used to model the irradiance in strong turbulence channels, and the negative exponential distribution can be used

to describe the saturated irradiance fluctuations [22].

1.3 Thesis Outline and Contributions

This thesis is arranged into five chapters. Chapter 1 presents a brief background and recent development of OWC. As the demand for bandwidth and capacity increases, OWC becomes a promising alternative technology for both indoor and outdoor applications. However, the signal scintillation introduced by atmospheric turbulence is one of the greatest challenges encountered in OWC systems. To evaluate the performance of OWC systems, it is imperative to analyze the performance of BLER over different atmospheric turbulence models.

Chapter 2 provides detailed technical background for the entire thesis. Firstly, we introduce some basic modulation techniques. Most practical OWC systems are based on the IM/DD scheme. There are three popular modulation techniques: OOK, PPM, and SIM. However, we will mainly focus on SIM OWC in the following Chapters. Secondly, we present and classify four atmospheric turbulence models, namely, lognormal, Gamma-Gamma, K-distributed and negative exponential turbulence channels. Finally, the basic concepts of block error rate are introduced.

In Chapter 3, we analyze the BLER performance of different digital modulations over the Gamma-Gamma family turbulence models. We perform the BLER for noncoherent frequency shift keying (NCFSK) and DPSK modulations. In terms of binary phase shift keying modulation (BPSK), we consider approximation of the Gaussian Q-function in order to simplify the BLER. We propose to approximate the Gaussian Q-function using a sum of three exponentials with the trapezoidal rule. The BLER is derived for NCFSK/DPSK over the Gamma-Gamma turbulence channels using a series approach. A detailed truncation error analysis is also presented. Finally, we perform the asymptotic error rate analysis to examine the behavior of BLER.

In Chapter 4, we analyze the performance of BLER of SIM systems over the lognormal tur-

bulence models assuming NCFSK/DPSK and BPSK modulations. Gauss-Laguerre quadrature approach is used to approximate the BLER because it is challenging to derive the closed-form expression of BLER.

Chapter 5 summarizes the whole thesis and lists our contributions in this work. In addition, future work related to our current research is suggested.

Chapter 2

Modulation Techniques and Channel Modeling

In this Chapter, several digital modulation techniques for outdoor OWC applications are introduced first. The SIM will be described in great details. Several important turbulence channel models used to describe the probability density function (PDF) of the irradiance fluctuation are discussed. Finally, we will introduce basic concept of BLER, which will be employed as the performance metric for this thesis.

2.1 Modulation Techniques

A number of digital modulation techniques have been proposed for OWC over atmospheric turbulence channels. These modulation techniques include OOK, PPM and SIM. When choosing a modulation scheme, power efficiency, bandwidth efficiency, and design complexity of both the transmitter and the receiver are all important factors to consider. OOK is the most commonly used modulation technique for OWC systems due to its simplicity of design and implementation. However, an OOK with optimum error rate performance requires time-varying adaptive thresholds, and thus perfect knowledge of instantaneous channel state information is required. The PPM has advantage over the OOK in a sense that the PPM does not require adaptive detection thresholds. Moreover, the PPM has enhanced power efficiency compared to the OOK. The drawback is that the PPM has a complex transceiver design due to tight synchronization requirements and has higher bandwidth requirements. Recently, the SIM was

introduced as an attractive alternative to the OOK because it does not require adaptive detection thresholds, and the SIM has lower bandwidth requirement than the PPM. For this reason, in this thesis, we will mainly focus on the SIM as the digital modulation for our OWC study.

2.1.1 On-Off Keying

OOK is a widely used digital modulation technique for OWC with IM/DD due to its simplicity. The transmission of an optical pulse which occupies part of or entire bit duration represents a data bit "1", while the absence of an optical pulse represents a data bit "0". The OOK includes return-to-zero (RZ) and non-return-to-zero (NRZ) pulse formats. For the RZ scheme, a pulse with duration which only occupies a part of the bit duration is transmitted to represent "1"; however, the pulse duration is equal to the bit duration in the NRZ scheme. The RZ-OOK has improved power efficiency over the NRZ-OOK at the expense of increased bandwidth [23]. Nevertheless, the NRZ-OOK is used in most commercial OWC systems.

2.1.2 Pulse Position Modulation

The PPM is an alternative digital modulation to the OOK, and it has improved power efficiency. However, PPM requires higher bandwidth and greater implementation complexity. One characteristic of the PPM is the elimination of decision threshold dependence on the input signal power. In PPM, every pulse is used to represent one or more bits of a pulse with constant power accounting for one slot. The pulse position is determined according to the decimal value of the $\log_2 M$ data bits, where M is the cardinality of the symbol set. Therefore, the information bits are encoded by the pulse position for each symbol. In order to demodulate the information bits, both slot and symbol synchronization are required at the PPM receiver. However, tight timing synchronization requirement is one key drawback of the PPM. Because the data detection is based on the exact pulse position, timing jitters can significantly degrade its error rate performance. The PPM is mainly deployed in intersatellite OWC systems [10].

2.1.3 Subcarrier Intensity Modulation

In SIM systems, an RF signal $s(t)$, which is pre-modulated with the data source and properly biased, is used to modulate the irradiance of a continuous wave optical beam at the transmitter laser. We normalize the power of $s(t)$ to be unity. At the receiver, the photodetector converts the received optical intensity to an electrical signal through direct detection. The photocurrent at the output of photodetector can be written as [24]

$$i(t) = RI(t)A[1+\xi s(t)] + n(t) = RI(t)A[1+\xi\cos(\omega t+\phi)] + n(t) \tag{2.1}$$

where R is the photodetector responsivity, $I(t)$ is assumed to be a stationary random process describing the irradiance fluctuation caused by the atmospheric turbulence, A is the photodetector area, ω represents the frequency of the RF subcarrier signal, the phase $\phi \in (0,\pi)$ denotes the bit information, $n(t)$ is an additive white Gaussian noise (AWGN) process due to thermal and/or background noise, and ξ is the modulation index satisfying $-1 < \xi s(t) < 1$ in order to avoid overmodulation. Assuming the sample time is t_0, then the sample $I(t_0)$ at the time instant $t = t_0$ is a random variable (RV) I. The instantaneous signal-to-noise ratio (SNR) at the input of the electrical demodulator is given by [25]

$$\gamma = \frac{\text{Instantaneous signal power}}{\text{Total noise power}} = \frac{(RA\xi)^2}{\sigma^2}I^2 = \frac{(RA\xi)^2}{\sigma_s^2+\sigma_b^2+\sigma_t^2}I^2 \tag{2.2}$$

where σ^2 is the total noise variance, σ_s^2 denotes the variance of the shot noise induced by the intended optical signal, σ_b^2 represents the variance of the ambient light induced shot noise, and σ_t^2 stands for the variance of the thermal noise. For a practical receiver using a p-i-n photodiode, the ambient induced shot noise and the thermal noise dominate the performance of the receiver, i.e., $\sigma_b^2 \gg \sigma_s^2$ and $\sigma_t^2 \gg \sigma_s^2$. Therefore, we can neglect the signal induced shot

noise component. Then the instantaneous SNR becomes [24, eq. (4)]

$$\gamma = \frac{(RA\xi)^2}{\sigma_b^2 + \sigma_t^2} I^2 = \frac{(RA\xi)^2}{2\Delta f(qRI_b + 2k_b T_k / R_L)} I^2 \tag{2.3}$$

where I_b is the background light irradiance, q is the electronic charge, Δf is the noise equivalent bandwidth of the photodetector, k_b is the Boltzmann's constant, T_k is the temperature in Kelvin, and R_L is the load resistance.

An alternative definition of SNR is the electrical SNR, which is defined as [15]

$$\gamma_e = \frac{(RA\xi)^2}{\sigma^2} I^2 = \bar{\gamma} I^2 \tag{2.4}$$

where $\bar{\gamma}$ is the average electrical SNR under the assumption of $E[I] = 1$.

2.2 The Atmospheric Turbulence Models

In this section, we will introduce some background knowledge of several widely used atmospheric turbulence models. For outdoor OWC, several statistical models have been proposed to describe the irradiance fluctuation. The lognormal is widely used to describe the weak turbulence channels [26]. The Gamma-Gamma distribution has recently emerged as a useful turbulence model because it provides a good fit to the experimental measurements of irradiance for both weak and strong turbulence channels [16]. As the special cases of the Gamma-Gamma model, the K-distribution is commonly used to model the irradiance in strong turbulence regimes, and the negative exponential distribution can be used to describe the saturation regimes [22].

2.2.1 Lognormal Turbulence Model

The optical irradiance can be modeled as the lognormal distribution when the optical signal is propagated through an atmospheric turbulence channel with several hundred meters link

distance in a clear sky environment [19]. For a lognormal turbulence channel, the optical irradiance I is given by

$$I = k\exp(X), \;\; k > 0 \tag{2.5}$$

where k is a positive scalar, and X is a Gaussian RV with mean μ and variance σ^2. In OWC, the scintillation level σ has typical values between 0.02 and 0.5 [5], and it can never be greater than 0.75 [27]. The lognormal RV I has the PDF [20]

$$f_L(I) = \frac{1}{\sqrt{2\pi}\sigma I}\exp\left[-\frac{(\ln I - \mu)^2}{2\sigma^2}\right], \;\; I > 0 \tag{2.6}$$

where μ is a log-scale parameter defined as $\mu = \log k$. The nth moment of the lognormal PDF is $E[I^n] = k^n e^{n^2\sigma^2/2}$ [7]. With a normalized mean, i.e., $E[I] = 1$, one has $k = \exp(-\sigma^2/2)$, and the PDF of I can be re-written as

$$f_L(I) = \frac{1}{\sqrt{2\pi}\sigma I}\exp\left[-\frac{(\ln I + \sigma^2/2)^2}{2\sigma^2}\right], \;\; I > 0. \tag{2.7}$$

The PDF of inrradiance I is shown in Figure 2.1 for several different values of σ^2. From the definition in (1.3), the scintillation index for lognormal distributed irradiance is

$$\sigma_I^2 = \frac{E[I^2]}{(E[I])^2} - 1 = k^2 e^{n^2\sigma^2/2} - 1 = \exp(\sigma^2) - 1. \tag{2.8}$$

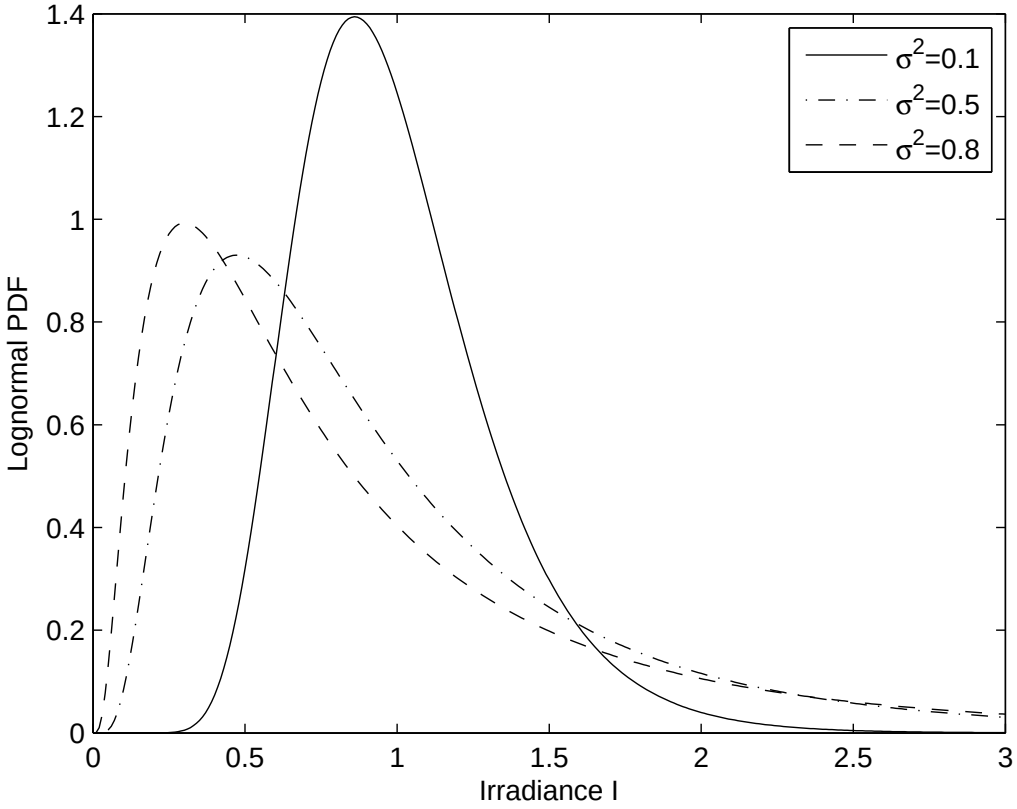

Figure 2.1: Lognormal probability density function for optical irradiance with variances $\sigma^2 = 0.1, 0.5, 0.8$.

2.2.2 Gamma-Gamma Turbulence Model

For a wide range of turbulence conditions (weak to strong), the Gamma-Gamma turbulence model has recently emerged as a useful turbulence model for OWC applications. Andrews *et al*. first proposed this model based on the modulation process that the fluctuation of light radiation propagating through the turbulent atmosphere is due to the large-scale and small-scale atmospheric effects [18]. The small-scale contributions to scintillation are according to the turbulent cells smaller than the Fresnel zone $R_F = (L/k)^{1/2}$ or the coherence radius ρ_0 of the optical wave, whichever is smaller. Here, L is the propagation path length between transmitter and receiver, k is the optical wave number. On the other hand, the large-scale fluctuations are generated by turbulent cells larger than that of the first Fresnel zone or the scattering disk $\frac{L}{k\rho_0}$,

whichever is larger [16]. The scattering disk is defined by the refractive cell size l at which the focusing angle $\theta_F \approx l/L$ is equal to the average diffraction angle $\theta_D \approx \frac{1}{k\rho_0}$ [28]. The small-scale cells are assumed to be modulated by the large-scale cells. For Gamma-Gamma distributed irradiance, the irradiance of the received optical wave is defined as a product of $I = I_x I_y$, where I_x and I_y are two statistically independent random variables, and arise from large-scale and small-scale turbulent cells, respectively. Both of them obey the Gamma distribution with PDFs given by [16]

$$P(I_x) = \frac{\alpha(\alpha I_x)^{\alpha-1}}{\Gamma(\alpha)} \exp(-\alpha I_x), \;\; I_x > 0, \;\; \alpha > 0 \tag{2.9}$$

and

$$P(I_y) = \frac{\beta(\beta I_y)^{\beta-1}}{\Gamma(\beta)} \exp(-\beta I_y), \;\; I_y > 0, \;\; \beta > 0 \tag{2.10}$$

where the positive parameters α and β are, respectively, the effective number of large-scale and small-scale cells of the scattering environment. By fixing I_x and using a change of variable, $I_y = I/I_x$, we obtain the conditional PDF

$$P(I \mid I_x) = \frac{\beta(\beta I/I_x)^{\beta-1}}{I_x\Gamma(\beta)} \exp(-\beta I/I_x), \;\; I > 0 \tag{2.11}$$

in which I_x is the conditional mean value of I. To obtain the unconditional irradiance distribution, we average (2.11) over the Gamma distribution of (2.9) and obtain the Gamma-Gamma PDF as

$$f_{GG}(I) = \int_0^\infty P(I \mid I_x)P(I_x)dI_x = \frac{2}{\Gamma(\alpha)\Gamma(\beta)}(\alpha\beta)^{\frac{\alpha+\beta}{2}} I^{\frac{\alpha+\beta}{2}-1} K_{\alpha-\beta}(2\sqrt{\alpha\beta I}), \;\; I > 0 \tag{2.12}$$

where $\Gamma(\cdot)$ denotes the Gamma function, and $K_{\alpha-\beta}(\cdot)$ is the modified Bessel function of the second kind of order $\alpha-\beta$. Assuming plane wave propagation, α and β can be defined as [15]

$$\alpha = \left[\exp\left(\frac{0.49\sigma_p^2}{\left(1+1.11\sigma_p^{12/5}\right)^{7/6}} \right) - 1 \right]^{-1} \tag{2.13}$$

and

$$\beta = \left[\exp\left(\frac{0.51\sigma_p^2}{\left(1+0.69\sigma_p^{12/5}\right)^{5/6}} \right) - 1 \right]^{-1}. \tag{2.14}$$

On the other hand, if we assume spherical wave propagation, the parameters α and β are given by [6], [15]

$$\alpha = \left[\exp\left(\frac{0.49\sigma_l^2}{\left(1+0.18d^2+0.56\sigma_l^{12/5}\right)^{7/6}} \right) - 1 \right]^{-1} \tag{2.15}$$

and

$$\beta = \left[\exp\left(\frac{0.51\sigma_l^2 \left(1+0.69\sigma_l^{12/5}\right)^{-5/6}}{\left(1+0.9d^2+0.62d^2\sigma_l^{12/5}\right)^{5/6}} \right) - 1 \right]^{-1} \tag{2.16}$$

where $d = (kD^2/4L)^{1/2}$, D is the diameter of the receiver collecting lens aperture. Under the assumption of plane wave and negligible inner scale, the inequality $\alpha > \beta$ always holds for OWC applications [29]. Without loss of generality, this inequality condition is assumed to be true in this work. From the Gamma-Gamma PDF in (2.12) , we find

$$E[I^2] = (1+1/\alpha)(1+1/\beta). \tag{2.17}$$

According to the PDFs of I_x and I_y in (2.9) and (2.10), the second moment of the irradiance I is

$$E[I^2] = E[I_x^2]E[I_y^2] = (1+\sigma_x^2)(1+\sigma_y^2) \tag{2.18}$$

where σ_x^2 and σ_y^2 represent the normalized variances of I_x and I_y, respectively. Normalizing $E[I] = 1$, using (1.3) and (2.18), the scintillation index becomes

$$\sigma_I^2 = (1+\sigma_x^2)(1+\sigma_y^2) - 1 = \sigma_x^2 + \sigma_y^2 + \sigma_x^2\sigma_y^2. \tag{2.19}$$

From (2.17) and (2.18), we use the following relationships

$$\alpha = \frac{1}{\sigma_x^2}, \;\; \beta = \frac{1}{\sigma_y^2} \tag{2.20}$$

to express the scintillation index as

$$\sigma_I^2 = \frac{1}{\alpha} + \frac{1}{\beta} + \frac{1}{\alpha\beta}. \tag{2.21}$$

The PDF in (2.12) can be alternatively expressed in series with the aid of a series expansion of the modified Bessel function [30, eq. (6)]

$$K_\nu(x) = \frac{\pi}{2\sin(\pi\nu)} \sum_{p=0}^{\infty} \left[\frac{(x/2)^{2p-\nu}}{\Gamma(p-\nu+1)p!} - \frac{(x/2)^{2p+\nu}}{\Gamma(p+\nu+1)p!} \right] \tag{2.22}$$

where $\nu \notin \mathbb{Z}$ ($\mathbb{Z}$ is the set integers) and $|x| < \infty$. Substituting (2.22) into (2.12), we have

$$f_{GG}(I) = \sum_{p=0}^{\infty} \left[a_p(\alpha,\beta) I^{p+\beta-1} + a_p(\beta,\alpha) I^{p+\alpha-1} \right], \;\; I > 0 \tag{2.23}$$

where $(\alpha-\beta) \notin \mathbb{Z}$ and

$$a_p(x,y) = \frac{\pi(xy)^{p+y}}{\sin(\pi(x-y))\Gamma(x)\Gamma(y)\Gamma(p-x+y+1)p!}. \tag{2.24}$$

Using the Euler reflective identity $\pi/\sin(\pi(x-y)) = \Gamma(x-y)\Gamma(1-x+y)$ [31, eq. 8.334 (3)], we can rewrite (2.24) as

$$a_p(x,y) = \frac{(xy)^{p+y}\Gamma(x-y)\Gamma(1-x+y)}{\Gamma(x)\Gamma(y)\Gamma(p-x+y+1)p!}. \tag{2.25}$$

A plot of the Gamma-Gamma PDF is given in Fig. 2.2 for three representative turbulence conditions: $\alpha = 11.7, \beta = 10.1$ (weak), $\alpha = 4.1, \beta = 1.4$ (moderate), and $\alpha = 4.6, \beta = 1.2$ (strong), where the corresponding Rytov variance σ_p^2 are 0.2, 3, and 5, respectively. It can be shown that the distribution spreads out more when the turbulence increases from weak to strong, which implies an increase in the range of possible irradiance values.

2.2.3 K-distributed Turbulence Model

The K-distributed turbulence channel is another useful turbulence model describing irradiance fluctuations in strong turbulence conditions [18], [32], [33]. In OWC systems, if the normalized scintillation index is confined to the range $(2,3)$ or the propagation distance is approximately 1km, the resulting turbulence channel is characterized by a K-distributed model [34], which is a special case of the Gamma-Gamma model when $\beta = 1$. The PDF of a K-distributed RV I is [24, eq. (8)]

$$f_K(I) = \frac{2}{\Gamma(\alpha)}\alpha^{\frac{\alpha+1}{2}} I^{\frac{\alpha-1}{2}} K_{\alpha-1}(2\sqrt{\alpha I}), \;\; I > 0. \tag{2.26}$$

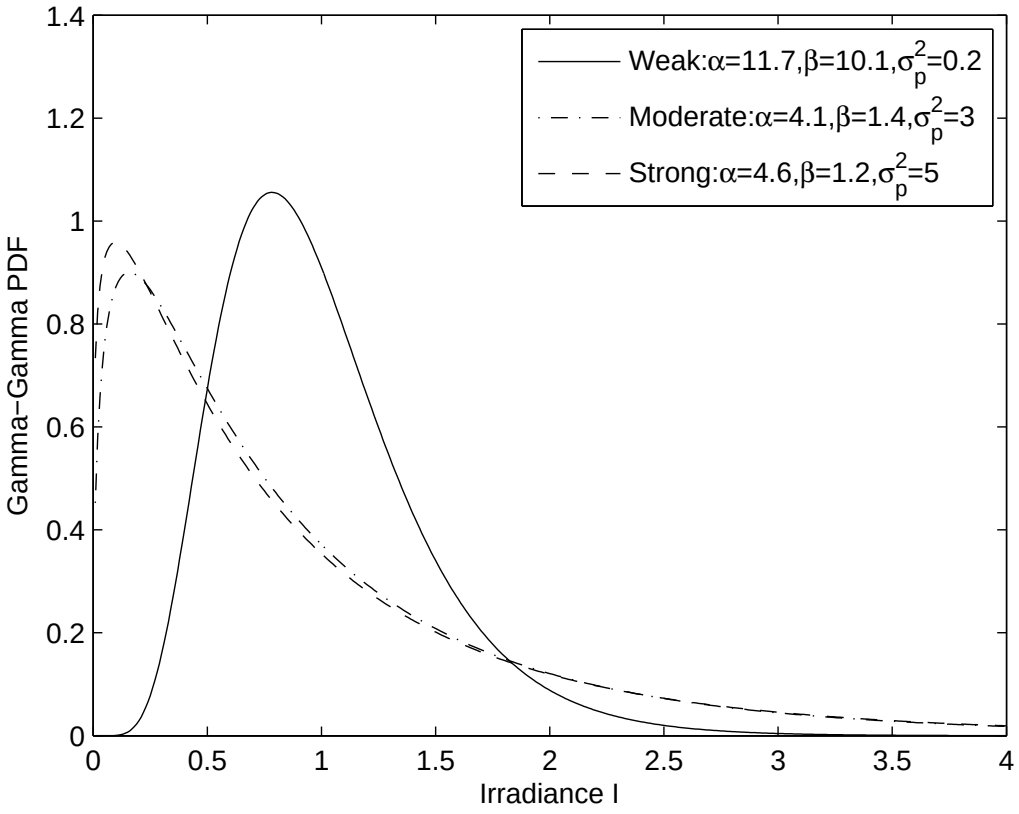

Figure 2.2: Gamma-Gamma probability density function for weak, moderate and strong turbulence regimes.

Alternatively, it can be written in a series form by letting $\beta = 1$ in (2.23) as

$$f_K(I) = \sum_{p=0}^{\infty} \left[a_p(\alpha,1) I^p + a_p(1,\alpha) I^{p+\alpha-1} \right], \quad I > 0. \tag{2.27}$$

The typical values of the parameter α lie within $(1,2)$ [35]. It is easily shown that the resulting scintillation index is

$$\sigma_I^2 = \frac{2}{\alpha} + 1. \tag{2.28}$$

2.2.4 Negative Exponential Turbulence Model

The negative exponential atmospheric turbulence channel is used to describe the limiting case of saturated scintillation [16], [13]. The PDF of the irradiance is given by

$$f_{NE}(I) = \frac{1}{I_0} \exp\left(-\frac{I}{I_0}\right), \quad I > 0 \tag{2.29}$$

where $E[I] = I_0$ is the mean received irradiance, and it is assumed to be unity. Thus we have

$$f_{NE}(I) = \exp(-I), \quad I > 0. \tag{2.30}$$

We will now show the negative exponential model is a special case of the K-distributed model. In the K-distributed turbulence model, the irradiance I can be considered as a product of two statistically independent RVs, $I = UV$, where U and V follow the exponential distribution and the Gamma distribution, respectively [14],[36]. Therefore, we have

$$f_U(u) = \exp(-u), \quad u > 0 \tag{2.31}$$

and

$$f_V(v) = \frac{\alpha^{\alpha} v^{\alpha-1}}{\Gamma(\alpha)} \exp(-\alpha v), \;\; v > 0 \tag{2.32}$$

where α is the effective number of discrete refractive scatterers. By first fixing $V = v$ and writing $U = I/v$, we obtain the conditional PDF of RV I as

$$f_K(I \mid v) = \left(\frac{1}{v}\right) f_U\left(\frac{I}{v}\right) = \left(\frac{1}{v}\right) \exp\left(-\frac{I}{v}\right) \tag{2.33}$$

where v is the conditional mean value of I. When the parameter α approaches ∞, the PDF of Gamma RV given in (2.32) converges to the Dirac delta function located at 1, i.e.,

$$\lim_{\alpha\to\infty} f_V(v) = \delta(v-1). \tag{2.34}$$

Therefore, the PDF of K-distributed model can be written as

$$\begin{aligned} \lim_{\alpha\to\infty} f_K(I) &= \lim_{\alpha\to\infty} \int_0^{\infty} \left(\frac{1}{v}\right) \exp\left(-\frac{I}{v}\right) f_V(v) dv \\ &= \int_0^{\infty} \left(\frac{1}{v}\right) \exp\left(-\frac{I}{v}\right) \delta(v-1) dv \\ &= \exp(-I), \;\; I > 0. \end{aligned} \tag{2.35}$$

The negative exponential PDF is shown in Fig. 2.3 for different values of I_0.

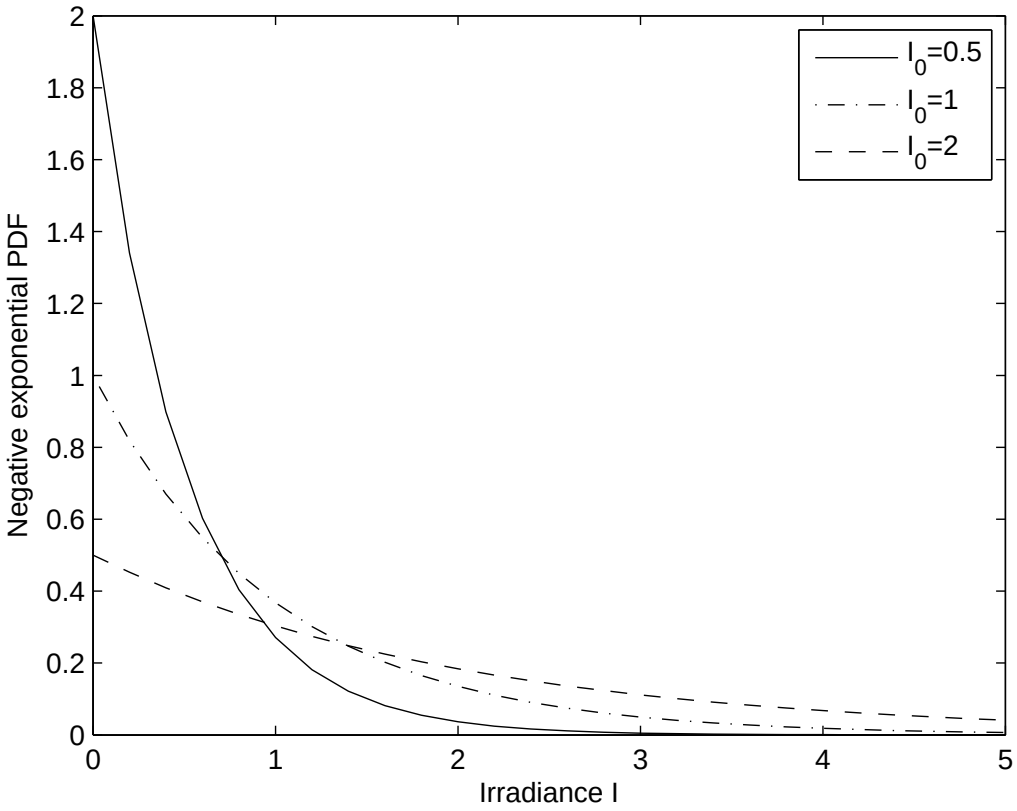

Figure 2.3: Negative exponential probability density function for $I_0 = 0.5, 1, 2$.

2.3 Probability of Block Error Rate

In OWC, the turbulence fading channel typically changes slowly. Despite the received optical intensity suffers from random fluctation, the coherence time of atmospheric turbulence channels is typically on the order of 1 msec, while the data rate of OWC systems can be on the order of Gbps [37]. Here, the channel coherence time is the time duration in which the channel can be considered as constant. As a result, the same channel fading coefficient will affect a large block of data bits. Therefore, the bit-errors will have dependance, i.e., the slow turbulence fading channel has memory. The traditional BER is inadequate to assess the performance of such system, and BLER is a more meaningful performance metric.

For a nonfading channel, the bit errors are independent and identically distributed, and the

errors in a block of N bits are binomially distributed. We denote $P(M,N)$ by the probability of block error rate or simply the block error, and it is defined as the probability of having more than M bit errors within a block of N bits. Thus, $P(M,N)$ is calculated by

$$P(M,N) = \sum_{m=M+1}^{N} \binom{N}{m} p^m (1-p)^{N-m} \tag{2.36}$$

where p is the probability of bit error.

Block error rate has several important applications. For examples, if a simple automatic repeat request system is used, the system performance is determined by the probability of occurrence of one or more bit errors in a block, i.e., $P(0,N)$. On the other hand, if an error-correction code is to be employed to correct up to M errors in each block of N bits, the system performance is governed by $P(M,N)$. In the special case when we set both M and N equal to 1, block error rate becomes the BER. Therefore, BLER is a generalized performance metric that is more suitable for slowly changing turbulence-induced fading channels.

In RF wireless communication literature, block error rate was studied for slow Rayleigh fading [38], and for slow Rayleigh fading with diversity reception [39]. Both works focused on noncoherent binary signalings, and did not treat the block error rate of binary phase shift keying. Despite most atmospheric fading channels are slowly changing, to our best knowledge, block error rate performance has not been studied for OWC systems in slow atmospheric turbulence channels.

Chapter 3

BLER Analysis for Gamma-Gamma Family Turbulence Models

In this Chapter, the block error performance of SIM OWC systems over the Gamma-Gamma family turbulence models will be analyzed. We compare four sum of exponentials approximations to the Gaussian Q-function, and choose the most suitable one to evaluate the average block error rate of SIM using BPSK modulation. The asymptotic error rate is presented to examine the behavior of block error rate in high SNR regimes.

The average block error rate for SIM over a slow fading channel can be written as

$$P(M,N) = \int_0^\infty P(M,N;\gamma) f(\gamma)\, d\gamma \tag{3.1}$$

where $P(M,N;\gamma)$ is the conditional block error probability, and $f(\gamma)$ denotes the PDF of the instantaneous SNR. Applying $\gamma = \bar{\gamma} I^2$ to (2.23), (2.27) and (2.30), the PDFs of the instantaneous SNR of the Gamma-Gamma, K-distributed and negative exponential channels can be obtained, respectively, as

$$f_{GG}(\gamma) = \frac{1}{2\sqrt{\gamma\bar{\gamma}}} \sum_{p=0}^{\infty} \left[a_p(\alpha,\beta) \left(\frac{\gamma}{\bar{\gamma}}\right)^{\frac{p+\beta-1}{2}} + a_p(\beta,\alpha) \left(\frac{\gamma}{\bar{\gamma}}\right)^{\frac{p+\alpha-1}{2}} \right] \tag{3.2}$$

and

$$f_K(\gamma) = \frac{1}{2\sqrt{\gamma\bar{\gamma}}} \sum_{p=0}^{\infty} \left[a_p(\alpha,1) \left(\frac{\gamma}{\bar{\gamma}}\right)^{\frac{p}{2}} + a_p(1,\alpha) \left(\frac{\gamma}{\bar{\gamma}}\right)^{\frac{p+\alpha-1}{2}} \right] \tag{3.3}$$

and

$$f_{NE}(\gamma) = \frac{1}{2\sqrt{\gamma\bar{\gamma}}} \exp\left(-\sqrt{\frac{\gamma}{\bar{\gamma}}}\right). \tag{3.4}$$

3.1 BLER for NCFSK/DPSK Modulation

The conditional probability of bit-error for noncoherent modulations is

$$p(\gamma) = \frac{1}{2} \exp(-\eta\gamma) \tag{3.5}$$

where $\eta = 1/2$ for NCFSK and $\eta = 1$ for DPSK.

For the Gamma-Gamma turbulence channel model, we substitute (2.36), (3.5), (3.2) into (3.1), and obtain the average block error rate as

$$\begin{aligned} P_{GG}^{nc}(M,N) = & \frac{1}{2} \sum_{m=M+1}^{N} \sum_{p=0}^{\infty} \binom{N}{m} \left[a_p(\alpha,\beta) \bar{\gamma}^{-\left(\frac{p+\beta}{2}\right)} \int_0^{\infty} \left(\frac{1}{2} e^{-\eta\gamma}\right)^m \left(1 - \frac{1}{2} e^{-\eta\gamma}\right)^{N-m} \right. \\ & \left. \times \gamma^{\frac{p+\beta-2}{2}} d\gamma + a_p(\beta,\alpha) \bar{\gamma}^{-\left(\frac{p+\alpha}{2}\right)} \int_0^{\infty} \left(\frac{1}{2} e^{-\eta\gamma}\right)^m \left(1 - \frac{1}{2} e^{-\eta\gamma}\right)^{N-m} \gamma^{\frac{p+\alpha-2}{2}} d\gamma \right]. \end{aligned} \tag{3.6}$$

Using the binomial expansion formula, we obtain

$$\left(\frac{1}{2} e^{-\eta\gamma}\right)^m \left(1 - \frac{1}{2} e^{-\eta\gamma}\right)^{N-m} = \sum_{k=0}^{N-m} \binom{N-m}{k} (-1)^k \left(\frac{1}{2}\right)^{m+k} e^{-(m+k)\eta\gamma}. \tag{3.7}$$

Substituting (3.7) into (3.6) and using an integral identity [31, eq. 3.326 (2.10)], which is

$$\int_0^{\infty} x^m \exp(-\beta x^n) dx = \frac{\Gamma(r)}{n\beta^r} \tag{3.8}$$

where $r = \frac{m+1}{n}$, we solve for the integral

$$\int_0^\infty \left(\frac{1}{2}e^{-\eta\gamma}\right)^m \left(1-\frac{1}{2}e^{-\eta\gamma}\right)^{N-m} \gamma^{\frac{p+x-2}{2}} d\gamma = \sum_{k=0}^{N-m} \binom{N-m}{k} (-1)^k \left(\frac{1}{2}\right)^{m+k} \times (\eta(m+k))^{-\frac{p+x}{2}} \Gamma\left(\frac{p+x}{2}\right). \tag{3.9}$$

Applying (3.9) to (3.6), we obtain a series solution to the average block error rate as

$$P_{GG}^{nc}(M,N) = \sum_{m=M+1}^{N} \sum_{k=0}^{N-m} \sum_{p=0}^{\infty} \binom{N}{m} \binom{N-m}{k} (-1)^k \left(\frac{1}{2}\right)^{m+k+1} \left[a_p(\alpha,\beta)\bar{\gamma}^{-\frac{p+\beta}{2}} [\eta(m+k)]^{-\frac{p+\beta}{2}} \times \Gamma\left(\frac{p+\beta}{2}\right) + a_p(\beta,\alpha)\bar{\gamma}^{-\frac{p+\alpha}{2}} [\eta(m+k)]^{-\frac{p+\alpha}{2}} \Gamma\left(\frac{p+\alpha}{2}\right)\right]. \tag{3.10}$$

The analytical result obtained in (3.10) is new, and it can be used to compute the block error rate of SIM systems employing noncoherent modulations over the Gamma-Gamma turbulence channels. The series solution in (3.10) is a converging series and a detailed proof is given in Appendix A.

Using (3.10), one can straightforwardly obtain the average block error rate over the K-distributed turbulence model by setting $\beta = 1$ as

$$P_{K}^{nc}(M,N) = \sum_{m=M+1}^{N} \sum_{k=0}^{N-m} \sum_{p=0}^{\infty} \binom{N}{m} \binom{N-m}{k} (-1)^k \left(\frac{1}{2}\right)^{m+k+1} \left[a_p(\alpha,1)\bar{\gamma}^{-\frac{p+1}{2}} [\eta(m+k)]^{-\frac{p+1}{2}} \times \Gamma\left(\frac{p+1}{2}\right) + a_p(1,\alpha)\bar{\gamma}^{-\frac{p+\alpha}{2}} [\eta(m+k)]^{-\frac{p+\alpha}{2}} \Gamma\left(\frac{p+\alpha}{2}\right)\right]. \tag{3.11}$$

For the negative exponential turbulence channel model, substituting (2.36) and (3.4) into

(3.1) and using the binomial expansion formula, we obtain the average block error rate as

$$\begin{aligned} P_{NE}^{nc}(M,N) &= \sum_{m=M+1}^{N} \binom{N}{m} \frac{1}{2\sqrt{\bar{\gamma}}} \int_0^{\infty} \left(\frac{1}{2}e^{-\eta\gamma}\right)^m \left(1-\frac{1}{2}e^{-\eta\gamma}\right)^{N-m} \exp\left(-\sqrt{\frac{\gamma}{\bar{\gamma}}}\right) \gamma^{-\frac{1}{2}} d\gamma \\ &= \sum_{m=M+1}^{N} \sum_{k=0}^{N-m} \binom{N}{m} \binom{N-m}{k} (-1)^k \left(\frac{1}{2}\right)^{m+k+1} \bar{\gamma}^{-\frac{1}{2}} \\ &\quad \times \int_0^{\infty} \exp\left(-\eta\gamma(m+k) - \sqrt{\frac{\gamma}{\bar{\gamma}}}\right) \gamma^{-\frac{1}{2}} d\gamma. \end{aligned} \tag{3.12}$$

We let $x = \sqrt{\gamma}$, then the integral part of (3.12) becomes

$$\int_0^{\infty} \exp\left(-\eta\gamma(m+k) - \sqrt{\frac{\gamma}{\bar{\gamma}}}\right) \gamma^{-\frac{1}{2}} d\gamma = 2\int_0^{\infty} \exp\left(-\eta(m+k)x^2 - \bar{\gamma}^{-\frac{1}{2}}x\right) dx. \tag{3.13}$$

To solve (3.13), using [31, eq. 3.322(2)], i.e.,

$$\int_0^{\infty} \exp\left(-\frac{x^2}{4\beta} - \gamma x\right) dx = \sqrt{\pi\beta}\exp(\beta\gamma^2)\left[1-\Phi(\gamma\sqrt{\beta})\right] \tag{3.14}$$

we simplify the integral in (3.12) and obtain a series solution for the negative exponential channel as

$$\begin{aligned} P_{NE}^{nc}(M,N) = \sum_{m=M+1}^{N} \sum_{k=0}^{N-m} \binom{N}{m} \binom{N-m}{k} (-1)^k \left(\frac{1}{2}\right)^{m+k} \sqrt{\frac{\pi}{\eta\bar{\gamma}(m+k)}} \\ \times \exp\left(\frac{1}{4\eta\bar{\gamma}(m+k)}\right) Q\left(\sqrt{\frac{1}{2\eta\bar{\gamma}(m+k)}}\right) \end{aligned} \tag{3.15}$$

where $Q(x) = \int_x^{\infty} \exp(-u^2/2)/\sqrt{2\pi}\,du$ is the Gaussian Q-function.

3.2 BLER for BPSK Modulation

For coherent BPSK modulation, the conditional bit-error rate is $p(\gamma) = Q(\sqrt{2\gamma})$. Substituting this bit-error rate into (2.36) and using the binomial expansion formula, the average block

error rate can be written as

$$P^c(M,N) = \int_0^\infty \sum_{m=M+1}^{N} \sum_{k=0}^{N-m} \binom{N}{m} \binom{N-m}{k} (-1)^k \left(Q(\sqrt{2\gamma})\right)^{m+k} f_\gamma(\gamma) d\gamma. \tag{3.16}$$

It is analytically challenging to find an exact expression from (3.16) because it involves integration of the $(m+k)$th power of the Gaussian Q-function. Therefore, we consider an approximation of the Gaussian Q-function to further evaluate the average probability of error.

In the wireless communication literature, there exist numerous approximations to the Gaussian Q-function. One analytically tractable approximation is the sum of exponentials approximation. The infinite sum of exponentials approximation is given by [40]

$$Q(x) = \lim_{N\to\infty} \frac{1}{N} \sum_{i=1}^{N} \frac{1}{2} e^{-\tilde{a}_i x^2} \tag{3.17}$$

where $\tilde{a}_i = (1/2)\sin^{-2}(\pi(i-1)/(2N-2))$, and this approximation is only accurate when N is asymptotically large. Recently, based on a Prony approximation approach, Loskot and Beaulieu proposed two new sum of exponentials approximations involving only two terms or three terms respectively as [40]

$$Q(x) \approx 0.208 e^{-0.971x^2} + 0.147 e^{-0.525x^2} \tag{3.18}$$

and

$$Q(x) \approx 0.168 e^{-0.876x^2} + 0.144 e^{-0.525x^2} + 0.002 e^{-0.603x^2}. \tag{3.19}$$

It was shown in [40] that both (3.18) and (3.19) can provide adequate approximation of the Gaussian Q-function without having a large number of exponential terms. Using an upper bound of the complementary error function $\mathrm{erfc}(x)$ and the trapezoidal rule, Chiani *et al*. pro-

posed the following two-term approximation [41]

$$Q(x) \approx \frac{1}{12}\exp\left(-\frac{1}{2}x^2\right) + \frac{1}{4}\exp\left(-\frac{2}{3}x^2\right). \tag{3.20}$$

Using a similar approach, we propose the following new sum of three exponentials approximation of the $Q(x)$ as

$$Q(x) \approx \frac{5}{24}\exp\left(-2x^2\right) + \frac{4}{24}\exp\left(-\frac{11}{20}x^2\right) + \frac{1}{24}\exp\left(-\frac{1}{2}x^2\right). \tag{3.21}$$

A detailed derivation of (3.20) and (3.21) are given as follows. The complementary error function is defined as

$$\text{erfc}(x) = \frac{2}{\sqrt{\pi}}\int_x^\infty e^{-t^2}dt \tag{3.22}$$

and the Gaussian Q-function can be expressed in terms of the $\text{erfc}(\cdot)$ as

$$Q(x) = \frac{1}{2}\text{erfc}\left(\frac{x}{\sqrt{2}}\right). \tag{3.23}$$

In the following, we will first focus on the approximation of $\text{erfc}(\cdot)$. From [42], we have the following integral of an exponential form for the $\text{erfc}(x)$ as

$$\text{erfc}(x) = \frac{2}{\pi}\int_0^{\pi/2}\exp\left(-\frac{x^2}{\sin^2\theta}\right)d\theta, \;\; x \geq 0. \tag{3.24}$$

It is observed that $\exp\left(-\frac{x^2}{\sin^2\theta}\right)$ is a monotonically increasing function in θ for $0 \leq \theta \leq \pi/2$. We can arbitrarily choose $N+1$ values of θ between 0 and $\pi/2$, $0 = \theta_0 \leq \theta_1 ... \leq \theta_N = \pi/2$, to obtain the following exponential upper bound as

$$\text{erfc}(x) \leq \frac{2}{\pi}\sum_{i=1}^{N}\int_{\theta_{i-1}}^{\theta_i}\exp\left(-\frac{x^2}{\sin^2\theta_i}\right)d\theta. \tag{3.25}$$

We choose $N = 2$ for an arbitrary point θ and use the trapezoidal rule, and obtain

$$\text{erfc}(x) \approx g(x,\theta) = \left(\frac{1}{2} - \frac{\theta}{\pi}\right)\exp(-x^2) + \frac{1}{2}\exp\left(-\frac{x^2}{\sin^2\theta}\right). \tag{3.26}$$

Parameter θ is chosen to minimize the integral of the relative error over a specified range $[0,R]$, i.e.,

$$\theta_{opt} = \arg\min_{\theta} \frac{1}{R}\int_0^R \frac{|g(x,\theta) - \text{erfc}(x)|}{\text{erfc}(x)}dx \tag{3.27}$$

where the optimum values are chosen in the range from 0 to $R = 13$ dB [41]. Substituting (3.24) and (3.26) into (3.27), the optimum value has been calculated numerically to be $\theta_{opt} \approx \pi/3$, leading to

$$\text{erfc}(x) \approx g(x,\theta_{opt}) = \frac{1}{6}\exp\left(-x^2\right) + \frac{1}{2}\exp\left(-\frac{4}{3}x^2\right). \tag{3.28}$$

In the case of $N = 3$, we let $\vec{\theta} = (\theta_1,\theta_2)^T$. Making a use of the trapezoidal rule, we obtain

$$\text{erfc}(x) \approx g(x,\vec{\theta}) = \frac{\theta_2}{\pi}\exp\left(-\frac{x^2}{\sin^2\theta_1}\right) + \left(\frac{1}{2} - \frac{\theta_1}{\pi}\right)\exp\left(-\frac{x^2}{\sin^2\theta_2}\right) + \left(\frac{1}{2} - \frac{\theta_2}{\pi}\right)\exp\left(-x^2\right). \tag{3.29}$$

To determine the optimum value in the same range $[0,R]$, we use the similar approach as in (3.27), i.e.,

$$\vec{\theta}_{opt} = \arg\min_{\theta_1,\theta_2} \frac{1}{R}\int_0^R \frac{\left|g(x,\vec{\theta}) - \text{erfc}(x)\right|}{\text{erfc}(x)}dx. \tag{3.30}$$

We substitute (3.24) and (3.29) into (3.30), we find $(\theta_1)_{opt} \approx \pi/6$ and $(\theta_2)_{opt} \approx 5\pi/12$. There-

fore, we obtain the following approximation

$$\mathrm{erfc}(x) \approx g(x, \vec{\theta}_{opt}) = \frac{5}{12}\exp\left(-4x^2\right) + \frac{1}{3}\exp\left(-\frac{11}{10}x^2\right) + \frac{1}{12}\exp\left(-x^2\right). \tag{3.31}$$

From (3.23), we derive the sum of two-term and three-term exponentials approximations of the Gaussian Q-function as (3.20) and (3.21), respectively.

To assess the accuracy of (3.18)-(3.21), we plot the relative error of these approximations in Fig. 3.1. Here, the relative error can be given by

$$e(x) = \frac{Q(x) - appro.Q(x)}{Q(x)} \tag{3.32}$$

where $appro.Q(x)$ is expressed as (3.18), (3.19), (3.20) and (3.21) in different cases. It is shown from Fig. 3.1 that none of (3.18)-(3.21) can provide a uniform accurate approximation to $Q(x)$. The Prony approximations in (3.18) and (3.19) can provide better approximation for a large argument especially when $x > 2$, while our new approximation in (3.21) is more accurate for small argument (e.g., $x < 1$) of $Q(x)$. Since the average error rate performance is a weighted average of $Q(x)$ with the respect to the fading PDF, the asymptotic large SNR error rate performance will largely depend on the behavior of the fading channel PDF near its origin [43]. Therefore, the accuracy of $Q(x)$ with smaller argument will play more significant role in the small error rate regime. For this reason, we will choose (3.21) to obtain a more accurate estimation of the block error rate for coherent BPSK signaling.

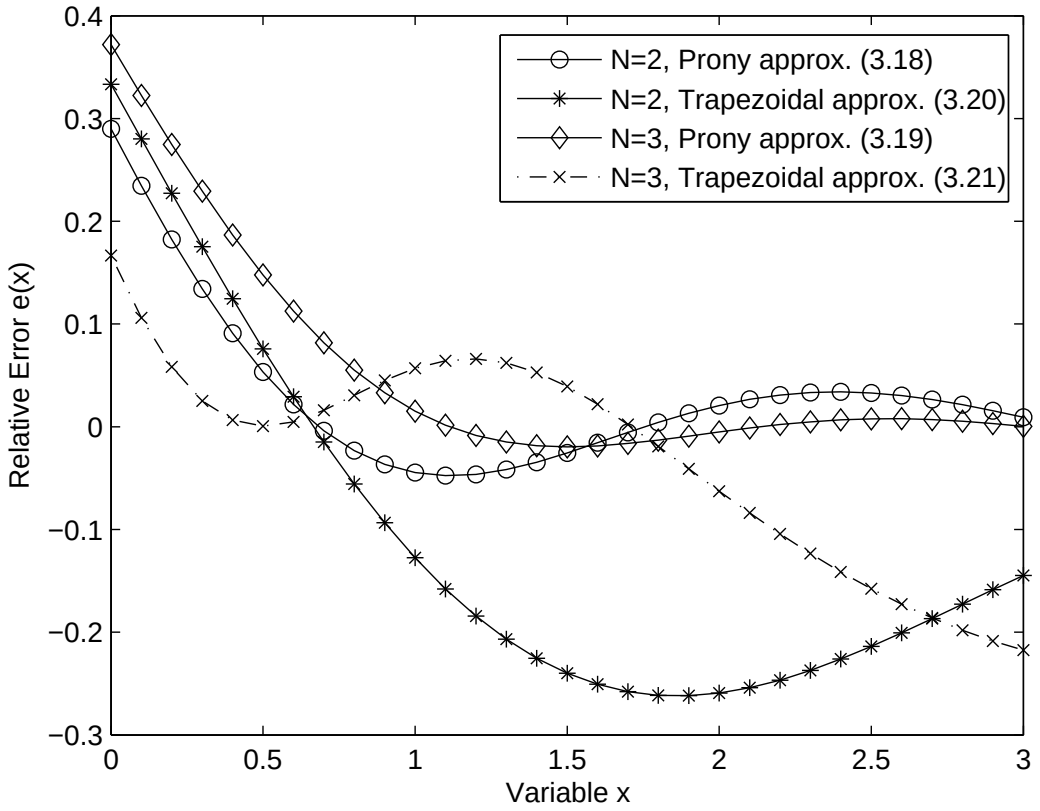

Figure 3.1: The relative error for various sum of exponentials approximations of the Gaussian Q-function.

Now substituting (3.21) into the Q-function of (3.16) and using the multinomial expansion formula, we have

$$\left(\frac{5}{24}e^{-4\gamma}+\frac{1}{6}e^{-11\gamma/10}+\frac{1}{24}e^{-\gamma}\right)^{m+k} = \sum_{t=0}^{m+k}\sum_{l=0}^{t}\binom{m+k}{t}\binom{t}{l}\left(\frac{1}{24}\right)^{m+k-t}\left(\frac{5}{24}\right)^{t-l}\left(\frac{1}{6}\right)^{l} \times \exp\left(-\gamma\left(m+k+3t-\frac{29}{10}l\right)\right). \tag{3.33}$$

Finally, substituting (3.2) and (3.33) into (3.16) and using [31, eq. 3.381(4)], we obtain a simplified series solution to the average block error rate of coherent BPSK in the Gamma-

Gamma turbulence channels as

$$P_{GG}^{c}(M,N) \approx \sum_{m=M+1}^{N} \sum_{k=0}^{N-m} \sum_{t=0}^{m+k} \sum_{l=0}^{t} \sum_{p=0}^{\infty} \binom{N}{m} \binom{N-m}{k} \binom{m+k}{t} \binom{t}{l} (-1)^k \frac{1}{2} \left(\frac{1}{24}\right)^{m+k-t} \times \left(\frac{5}{24}\right)^{t-l} \left(\frac{1}{6}\right)^{l} \left[a_p(\alpha,\beta) \bar{\gamma}^{-\frac{p+\beta}{2}} \left(m+k+3t-\frac{29}{10}l\right)^{-\frac{p+\beta}{2}} \Gamma\left(\frac{p+\beta}{2}\right) + a_p(\beta,\alpha) \bar{\gamma}^{-\frac{p+\alpha}{2}} \left(m+k+3t-\frac{29}{10}l\right)^{-\frac{p+\alpha}{2}} \Gamma\left(\frac{p+\alpha}{2}\right) \right]. \tag{3.34}$$

Similarly, we can obtain the average block error rate of coherent BPSK in K-distributed and negative exponential turbulence channels, respectively, as

$$P_{K}^{c}(M,N) \approx \sum_{m=M+1}^{N} \sum_{k=0}^{N-m} \sum_{t=0}^{m+k} \sum_{l=0}^{t} \sum_{p=0}^{\infty} \binom{N}{m} \binom{N-m}{k} \binom{m+k}{t} \binom{t}{l} (-1)^k \frac{1}{2} \left(\frac{1}{24}\right)^{m+k-t} \times \left(\frac{5}{24}\right)^{t-l} \left(\frac{1}{6}\right)^{l} \left[a_p(\alpha,1) \bar{\gamma}^{-\frac{p+1}{2}} \left(m+k+3t-\frac{29}{10}l\right)^{-\frac{p+1}{2}} \Gamma\left(\frac{p+1}{2}\right) + a_p(1,\alpha) \bar{\gamma}^{-\frac{p+\alpha}{2}} \left(m+k+3t-\frac{29}{10}l\right)^{-\frac{p+\alpha}{2}} \Gamma\left(\frac{p+\alpha}{2}\right) \right] \tag{3.35}$$

and

$$P_{NE}^{c}(M,N) \approx \sum_{m=M+1}^{N} \sum_{k=0}^{N-m} \sum_{t=0}^{m+k} \sum_{l=0}^{t} \binom{N}{m} \binom{N-m}{k} \binom{m+k}{t} \binom{t}{l} (-1)^k \bar{\gamma}^{-\frac{1}{2}} \left(\frac{1}{24}\right)^{m+k-t} \times \left(\frac{5}{24}\right)^{t-l} \left(\frac{1}{6}\right)^{l} \sqrt{\frac{\pi}{m+k+3t-29l/10}} \exp\left(\frac{1}{4\bar{\gamma}(m+k+3t-29l/10)}\right) \times Q\left(\sqrt{\frac{1}{2\bar{\gamma}(m+k+3t-29l/10)}}\right). \tag{3.36}$$

3.3 Asymptotic Error Rate Analysis

From the truncation error analysis (see Appendix A), we note that our series solution is increasingly accurate in high SNR regimes. Therefore, we can perform asymptotic error rate analysis to examine the behavior of error rate in high SNR regimes. Assuming $\alpha > \beta > 0$, so the term $\bar{\gamma}^{-\frac{p+\alpha}{2}}$ decreases faster than the term $\bar{\gamma}^{-\frac{p+\beta}{2}}$ in (3.10) for the same p value as the average SNR $\bar{\gamma}$ increases. Consequently, when $\bar{\gamma}$ approaches ∞, the second part of (3.10) can be neglected. Then, the block error rate of NCFSK/DPSK modulations in high SNR regimes can be approximated by

$$P^{nc}_{GG,asym} = \sum_{m=M+1}^{N} \sum_{k=0}^{N-m} \binom{N}{m} \binom{N-m}{k} (-1)^k \left(\frac{1}{2}\right)^{m+k+1} a_0(\alpha,\beta) \bar{\gamma}^{-\frac{\beta}{2}} [\eta(m+k)]^{-\frac{\beta}{2}} \Gamma\left(\frac{\beta}{2}\right). \tag{3.37}$$

Alternatively, the asymptotic BLER in (3.37) can be obtained by a Mellin transformation of the conditional BLER and the derivation is presented in Appendix B.

Similarly, the second part of (3.34) can be neglected as $\bar{\gamma}$ approaches ∞; therefore, the asymptotic block error rate of BPSK modulation can be expressed as

$$\begin{aligned} P^{c}_{GG,asym} = & \sum_{m=M+1}^{N} \sum_{k=0}^{N-m} \sum_{t=0}^{m+k} \sum_{l=0}^{t} \binom{N}{m} \binom{N-m}{k} \binom{m+k}{t} \binom{t}{l} (-1)^k \frac{1}{2} \left(\frac{1}{24}\right)^{m+k-t} \\ & \times \left(\frac{5}{24}\right)^{t-l} \left(\frac{1}{6}\right)^{l} a_0(\alpha,\beta) \bar{\gamma}^{-\frac{\beta}{2}} \left(m+k+3t-\frac{29}{10}l\right)^{-\frac{\beta}{2}} \Gamma\left(\frac{\beta}{2}\right). \end{aligned} \tag{3.38}$$

From (3.37) and (3.38), we observe the diversity order of both systems is $\frac{\beta}{2}$ or $\frac{1}{2}$ min (α,β), which is the same diversity order as the corresponding BER plots.

3.4 Numerical Results and Discussions

In this section, we compare the block error rate performance of SIM over different atmospheric turbulence models. The approximate block error rates are obtained by eliminating the

infinite terms after the first $L+1$ terms in the series solutions. We have chosen $L = 60$ for all numerical results. We consider weak ($\alpha = 3.78, \beta = 3.74$), moderate ($\alpha = 2.5, \beta = 2.06$), and strong ($\alpha = 2.04, \beta = 1.1$) turbulence conditions when describing the Gamma-Gamma turbulence models. The exact results are calculated by numerical integration using (2.36) and (2.12).

Figure 3.2 shows the block error rate for NCFSK over several representative block lengths. We compare the BLER in both fading and nonfading channels. This figure clearly shows the impact of turbulence fading on the BLER. The performance of block error rate under a nonfading channel improves rapidly with electrical SNR, while fading can degrade the BLER performance significantly. We also note a larger block length tends to give higher BLER.

In Fig. 3.3, block error rates are illustrated for NCFSK over the Gamma-Gamma channels with various turbulence conditions. The results demonstrate excellent agreement between the exact block error rates and our series solutions. We also observe that the asymptotic block error rate approaches the exact block error rate faster for strong turbulence condition ($\alpha = 2.04, \beta = 1.10$). This is because the asymptotic block error rates are determined only by the smaller channel parameter β at high SNR level.

In Fig. 3.4, we present block error rates for NCFSK over the K-distributed turbulence channels with different α values. The results also show excellent agreement between the exact block error rates and the series solutions with $L = 60$, where the exact block error rate is calculated by numerical integration of (2.36) and (2.26). We observe that the slope of K-distributed models is $-1/2$ which is determined by $\beta = 1$.

Figure 3.5 illustrates block error rates for NCFSK over the negative exponential turbulence channel. Here, we set $\alpha \to \infty$ and $\beta = 1$. The series solution consists of the exponential function and the Gaussian Q-function, which can simplify the integral of the average block error rate. From this figure, the results show excellent agreement between the exact block error rate and the series solution.

Figure 3.6 demonstrates the block error rate of BPSK signalling over the Gamma-Gamma

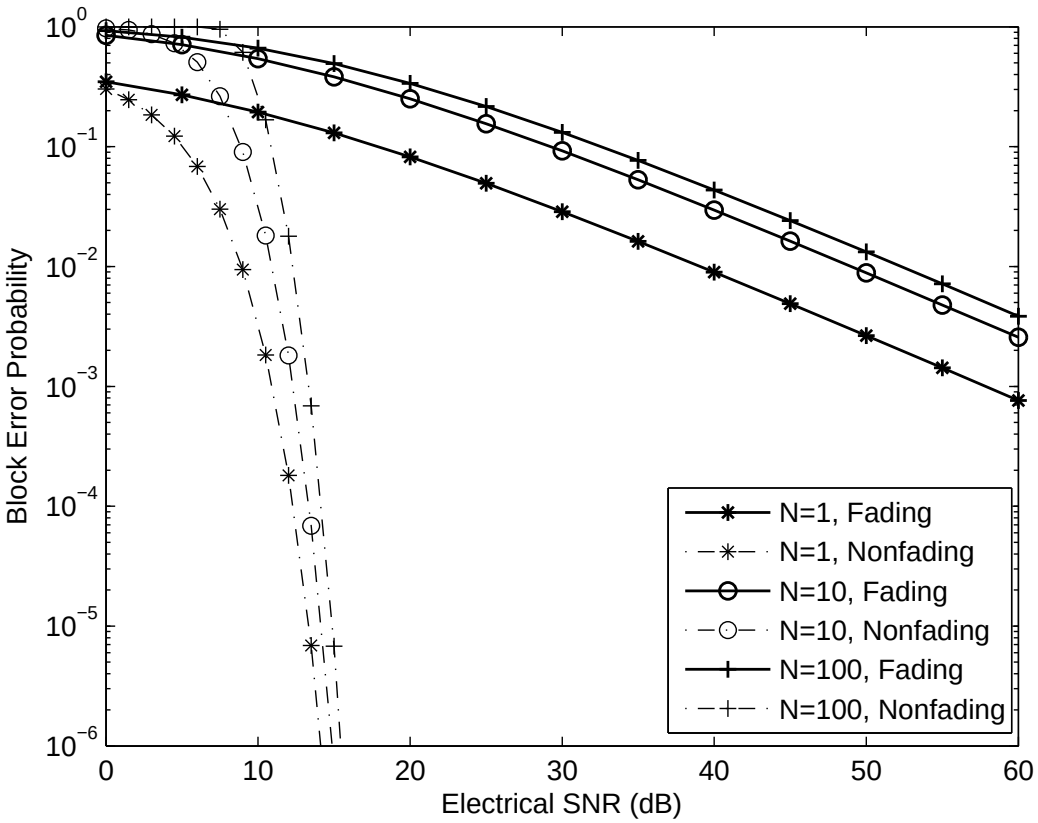

Figure 3.2: The block error rate of NCFSK, $P_{GG}^{nc}(0,N)$, over an unfaded channel and a faded Gamma-Gamma channel when $\alpha = 2.04, \beta = 1.10$.

channels. Again, our approximate solutions have excellent agreement with the exact block error rate when we make a use of the three-term approximation of the Gaussian Q-function in (3.33). As expected, the block error rate performance is better for the weak turbulence condition. For example, when SNR = 30 dB, the block error rate is at 7×10^{-4} for $\alpha = 3.78, \beta = 3.74$, and this BLER degrades to 5×10^{-2} under a strong turbulence environment for $\alpha = 2.50, \beta = 2.06$.

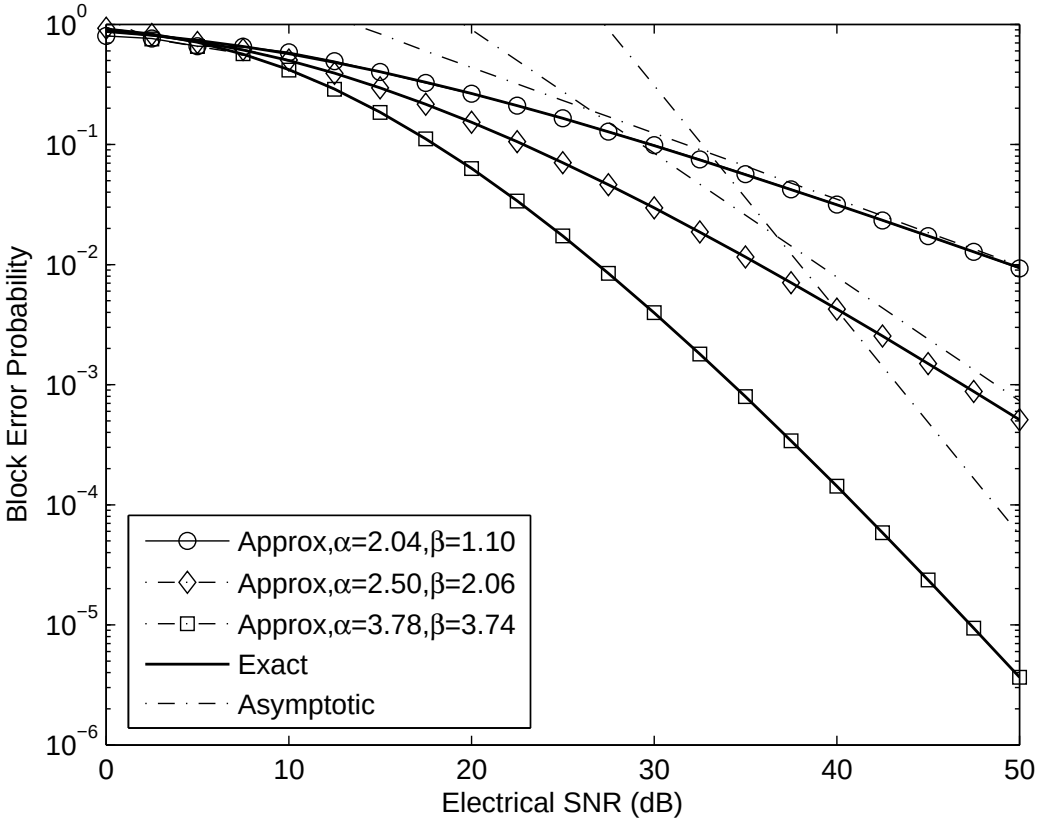

Figure 3.3: The block error rate of NCFSK, $P_{GG}^{nc}(2,53)$, over the Gamma-Gamma channels with different turbulence conditions.

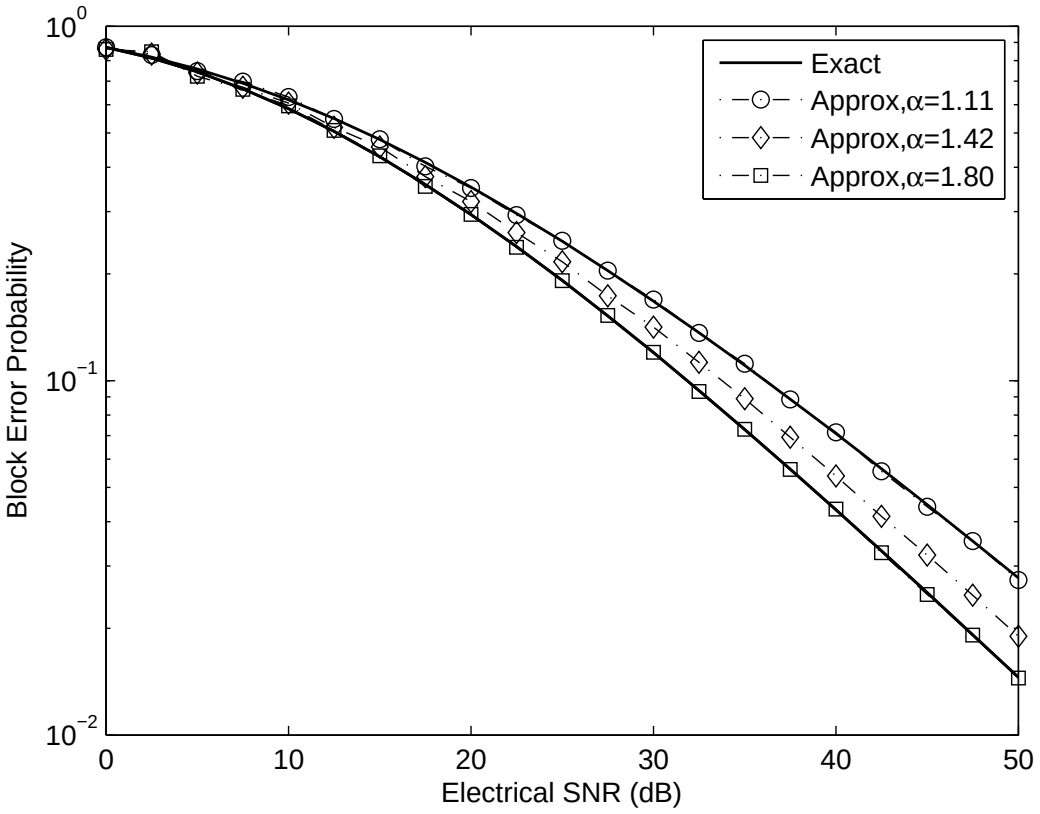

Figure 3.4: The block error rate of NCFSK, $P_K^{nc}(2,53)$, over the K-distributed channels with different turbulence conditions.

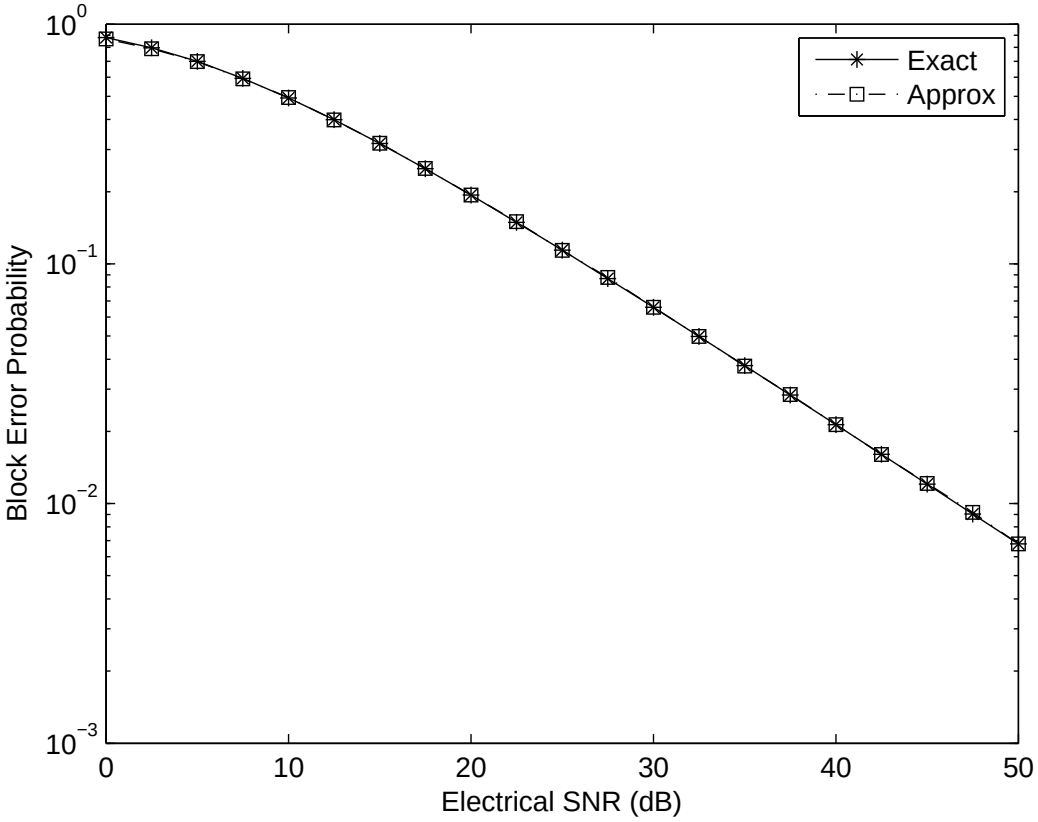

Figure 3.5: The block error rate of NCFSK, $P_{NE}^{nc}(2,53)$, over the negative exponential turbulence channel.

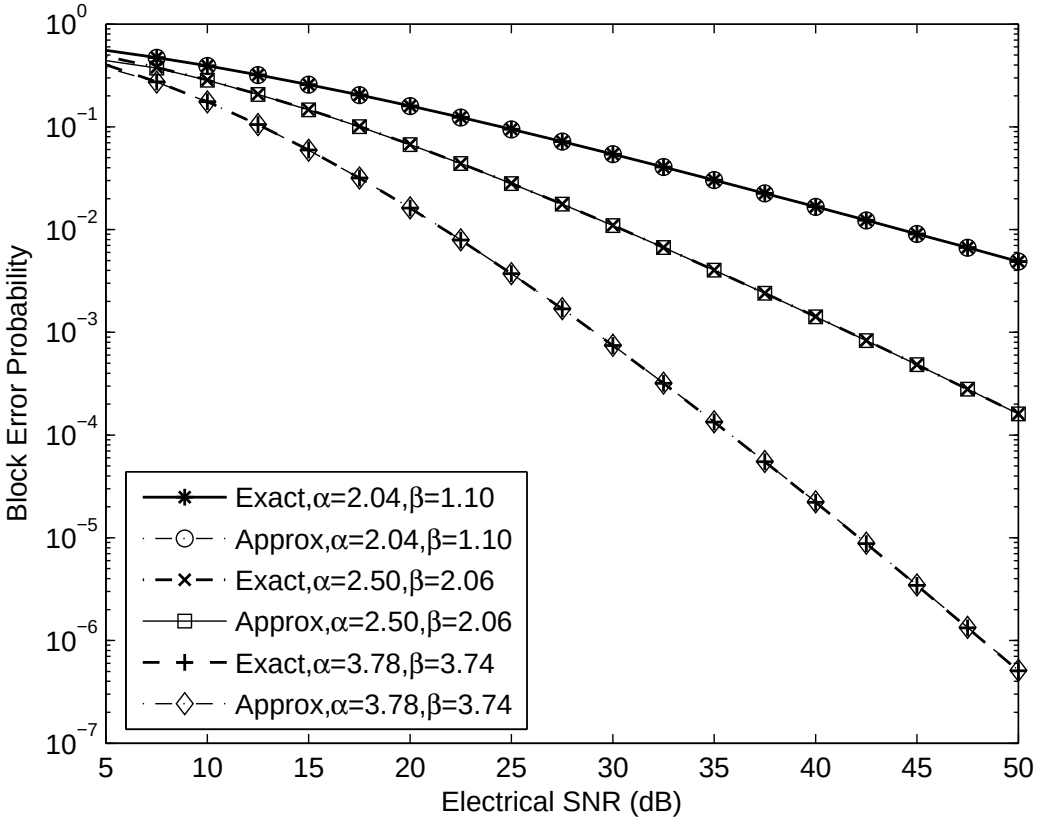

Figure 3.6: The block error rate of BPSK signalling, $P^{c}_{GG}(2,53)$, over the Gamma-Gamma channels with different turbulence conditions.

Chapter 4

BLER Analysis for Lognormal Turbulence Models

In this Chapter, the block error rate performance will be presented in an atmospheric turbulent channel based on the lognormal model. The NCFSK and DPSK modulated subcarrier will first be considered, and this will be followed by the BPSK modulation.

To analyze the average block error rate over the lognormal turbulence model, we need to use the similar approach as to that used in Gamma-Gamma family turbulence models to obtain the PDF of the instantaneous SNR. We have known that the PDF of the optical irradiance I for the lognormal turbulence channel can be expressed as (2.7). Applying $\gamma = \bar{\gamma} I^2$ into (2.7), we obtain the PDF of the instantaneous SNR for lognormal turbulence model as

$$f_L(\gamma) = \frac{1}{2\sqrt{2\pi}\sigma\gamma} \exp\left(-\frac{\left(\ln\left(\frac{\gamma}{\bar{\gamma}}\right) + \sigma^2 \right)^2}{8\sigma^2} \right) \tag{4.1}$$

which is another lognormal PDF. Since the exact BLER analysis involving the lognormal turbulence channel is analytically intractable, we propose to use the Gauss-Laguerre quadrature integration method to obtain an accurate estimation of BLER.

4.1 BLER for NCFSK/DPSK Modulation

In Chapter 3, we have the average block error rate expression in (3.1). Substituting (3.7) into (3.1), the block error rate over lognormal turbulence model can be written as

$$P_L^{nc}(M,N) = \sum_{m=M+1}^{N} \sum_{k=0}^{N-m} \binom{N}{m} \binom{N-m}{k} (-1)^k \left(\frac{1}{2}\right)^{m+k} \int_0^\infty \exp\left(-\gamma\eta(m+k)\right) f_L(\gamma) d\gamma. \tag{4.2}$$

To solve the integral in (4.2), a general solution for numerical calculation of the integrals in the form of $\int_0^\infty e^{-x} f(x)dx$ is presented in [44, eq. 25.4.45], which is

$$\int_0^\infty e^{-x} f(x)dx = \sum_{i=1}^{n} w_i f(x_i) + R_n \tag{4.3}$$

where n is the number of sample points used for approximation. The x_i is the ith zero of Laguerre polynomials $L_n(x)$, $w_i = \frac{x_i}{(n+1)^2[L_{n+1}(x_i)]^2}$ is the associated weights, and R_n is the reminder given by $\frac{(n!)^2}{(2n)!} f^{2n}(\xi)$. Note that $f^{2n}(\xi)$ is the $(2n)$th derivative of f, and ξ is some number between 0 and ∞. In general, the precise value of R_n is unknown, and the value is small enough so that it can be ignored. Thus the Gauss-Laguerre quadrature integral can be given by

$$\int_0^\infty e^{-x} f(x)dx \approx \sum_{i=1}^{n} w_i f(x_i). \tag{4.4}$$

Letting $x = \gamma[\eta(m+k)]$, we can rewrite the integral part of (4.2) as

$$\int_0^\infty e^{-\gamma\eta(m+k)} f_L(\gamma)d\gamma = \frac{1}{\eta(m+k)} \int_0^\infty e^{-x} f(x)dx \tag{4.5}$$

where $f(x) = \frac{\eta(m+k)}{\sqrt{8\pi}\sigma x} \exp\left(-\frac{\left[\ln\left(\frac{x}{\eta\bar{\gamma}(m+k)}\right)+\sigma^2\right]^2}{8\sigma^2}\right)$ according to (4.1).

Applying (4.4) to the right part of (4.5), we obtain

$$\int_0^\infty e^{-x} f(x)dx \approx \sum_{i=1}^{n} \frac{w_i}{\sqrt{8\pi}\sigma x_i} \exp\left(-\frac{\left[\ln\left(\frac{x_i}{\eta\bar{\gamma}(m+k)}\right)+\sigma^2\right]^2}{8\sigma^2} \right). \tag{4.6}$$

After substituting (4.6) into (4.2), we can approximate the block error rate of NCFSK/DPSK as

$$\begin{aligned} P_L^{nc}(M,N) \approx & \sum_{m=M+1}^{N} \sum_{k=0}^{N-m} \sum_{i=1}^{n} \binom{N}{m} \binom{N-m}{k} (-1)^k \left(\frac{1}{2}\right)^{m+k} \frac{w_i}{\sqrt{8\pi}\sigma x_i} \\ & \times \exp\left(-\frac{\left[\ln\left(\frac{x_i}{\eta\bar{\gamma}(m+k)}\right)+\sigma^2\right]^2}{8\sigma^2} \right). \end{aligned} \tag{4.7}$$

To calculate the above expression, Abramowitz *et al*. [44, table 25.9] provides a table of abscissas and weights up to $n = 20$. Therefore, we can easily obtain an approximation of the block error rate for NCFSK/DPSK modulation over the lognormal turbulence channels.

4.2 BLER for BPSK Modulation

To obtain the block error rate of coherent BPSK over the lognormal turbulence channels, we can also use the Gauss-Laguerre quaduature integration method. Substituting (3.33) into the Q-function of (3.16), we obtain the block error rate as

$$\begin{aligned} P_L^{c}(M,N) = & \sum_{m=M+1}^{N} \sum_{k=0}^{N-m} \sum_{t=0}^{m+k} \sum_{l=0}^{t} \binom{N}{m} \binom{N-m}{k} \binom{m+k}{t} \binom{t}{l} (-1)^k \left(\frac{1}{24}\right)^{m+k-t} \left(\frac{5}{24}\right)^{t-l} \\ & \times \left(\frac{1}{6}\right)^{l} \int_0^\infty \exp\left(-\gamma\left(m+k+3t-\frac{29}{10}l \right) \right) f_L(\gamma)d\gamma. \end{aligned} \tag{4.8}$$

Letting $x = \gamma(m+k+3t-29l/10)$ and using (4.4), we have

$$\begin{aligned}
&\int_0^\infty \exp\left(-\gamma\left(m+k+3t-\frac{29}{10}l\right)\right) f_L(\gamma)d\gamma \\
&\quad = \int_0^\infty e^{-x} f(x)dx \\
&\quad \approx \sum_{i=1}^{n} \frac{w_i}{\sqrt{8\pi}\sigma x_i} \exp\left(-\frac{\left[\ln\left(\frac{x_i}{\bar{\gamma}(m+k+3t-29l/10)}\right)+\sigma^2\right]^2}{8\sigma^2}\right)
\end{aligned} \tag{4.9}$$

where $f(x) = \frac{1}{\sqrt{8\pi}\sigma x} \exp\left(-\frac{\left[\ln\left(\frac{x}{\bar{\gamma}(m+k+3t-29l/10)}\right)+\sigma^2\right]^2}{8\sigma^2}\right)$. Substituting (4.9) into (4.8), we obtain the following approximate block error rate of BPSK signaling as

$$\begin{aligned}
P_L^c(M,N) \approx \sum_{m=M+1}^{N} \sum_{k=0}^{N-m} \sum_{t=0}^{m+k} \sum_{l=0}^{t} \sum_{i=1}^{n} \binom{N}{m}\binom{N-m}{k}\binom{m+k}{t}\binom{t}{l}(-1)^k \left(\frac{1}{24}\right)^{m+k-t}\left(\frac{5}{24}\right)^{t-l} \\
\times \left(\frac{1}{6}\right)^{l} \frac{w_i}{\sqrt{8\pi}\sigma x_i} \exp\left(-\frac{\left[\ln\left(\frac{x_i}{\bar{\gamma}(m+k+3t-29l/10)}\right)+\sigma^2\right]^2}{8\sigma^2}\right).
\end{aligned} \tag{4.10}$$

4.3 Numerical Results and Discussions

In this section, the block error rate based on a Gauss-Laguerre quadrature approximation is plotted in Fig. 4.1 for the lognormal turbulence channel with $\sigma = 0.2$. Here we use the 5th-order Gauss-Laguerre approximation to achieve an accurate estimation of the exact block error rate for both NCFSK and BPSK modulations. Our approximation solutions agree well with the exact block error rates over a wide range of SNR values, where the exact result is obtained by numerical integrations of (2.36) and (4.1).

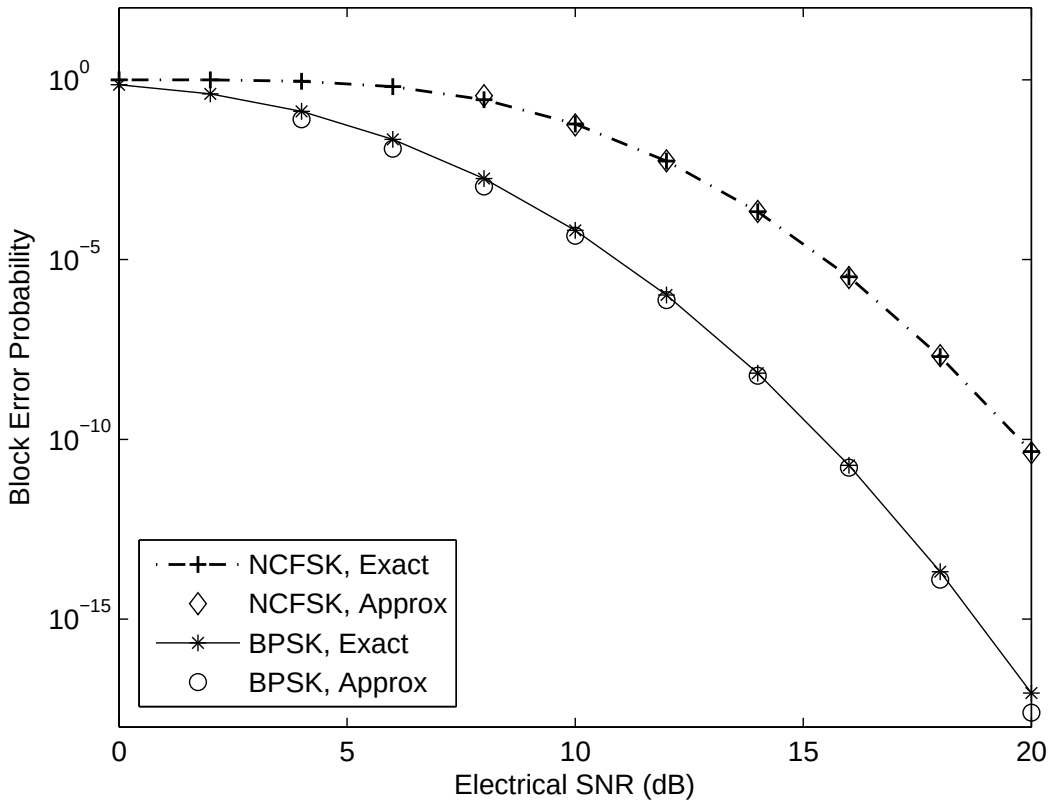

Figure 4.1: The block error rate of NCFSK and BPSK, $P_L^{nc}(2,53)$ and $P_L^{c}(2,53)$ over the log-normal channel with $\sigma = 0.2$ using a Laguerre polynomial of order $n = 5$.

Chapter 5

Conclusions

In this Chapter, we first summarize the contributions of this work, and then propose some future work related to this thesis.

5.1 Summary of Contributions

It is known that OOK is the most widely used signal modulation technique for OWC systems with IM/DD. However, the SIM is an attractive alternative to the OOK for data communication over atmospheric turbulence channels. Therefore, in this thesis, we have mainly analyzed the error rate performance of SIM based OWC systems. The BLER is a meaningful performance metric for OWC systems because the atmospheric turbulence channels typically change slowly, and the traditional BER is inadequate in evaluating the performance of such systems. The BLER performance has been studied extensively for SIM OWC systems employing various modulations over different atmospheric turbulence channels.

In Chapter 3, we have applied the PDF of the instantaneous SNR to three turbulence models (including the Gamma-Gamma, K-distributed, and negative exponential turbulence channels), and have derived the average block error rate for SIM using noncoherent binary modulations and coherent BPSK. For the BPSK modulation, we have proposed a new three-term approximation of the Gaussian Q-function to evaluate the average BLER of the SIM systems.

In Chapter 4, we have analyzed the BLER performance for NCFSK and BPSK modulations over the lognormal turubulence channels. Since the exact BLER analysis is analytically intractable, we have adopted the Gauss-Laguerre quadrature method to achieve an accurate

approximation of the exact BLER over the lognormal turbulence channels.

5.2 Future work

The Gaussian Q-function plays an important role in the performance analysis of digital communication systems. As shown in this thesis, it is difficult to obtain a closed-form expression of BLER for SIM-BPSK system because there exists no accurate approximation of high order Gaussian Q-function. The problem remains to find a highly accurate approximation of the Gaussian Q-function for a wide range of argument values. Such an improved approximation will facilitate the development of analytical expressions for the average block error probabilities.

Efficient numerical methods and infinite series solutions have been proposed for the calculation of the Gaussian Q-function [45]; however, these approximations are mathematically intractable. Recently, several new approximations of the Gaussian Q-function have been proposed in [41], [46]. A simple and useful approximation which involves the sum of two exponential functions was presented in [41]. These approximations were used to solve the problem of evaluating the average symbol error rate in fading channels. However, such approximation is not appropriate for small arguments of the Gaussian Q-function. Two approximations of the Gaussian Q-function were presented in [46] based on the geometric means of the upper bounds and the lower bounds. The first approximation is highly accurate but its mathematical form is intractable. The second one is simple but it does not guarantee sufficient accuracy.

In this thesis, we have compared four approximations of the Gaussian Q-function, while none of these approximations can provide a uniform of accuracy for all values of the Gaussian Q-function. Therefore, one possible future research topic is to develop novel, uniformly accurate, and tractable approximations to the high order Gaussian Q-function, and apply these new approximations to study the BLER for coherent modulations.

Bibliography

[1] F. R. Gfeller and U. Bapst, "Wireless in-house data communication via diffuse infrared radiation," *Proc. IEEE*, vol. 67, pp. 1474-1486, Nov. 1979.

[2] S. Qazi, "Challenges in outdoor and indoor optical wireless communications," *Int. Conf. on Wireless Networks*, pp. 448-458, 2006.

[3] V. W. S. Chan, "Free-space optical communications," *IEEE/OSA J. Lightw. Technol.*, vol. 24, pp. 4750-4762, Dec. 2006.

[4] D. C. O'Brien and M. Katz, "Optical wireless communication within fourth-generation wireless systems," *J. Opt. Netw.*, vol. 4, pp. 312-322, June. 2005.

[5] X. Zhu and J. M. Kahn, "Free-space optical communication through atmospheric turbulence channels," *IEEE Trans. Commun.*, vol. 50, pp. 1293-1300, Aug. 2002.

[6] M. Uysal, J. Li and M. Yu, "Error rate performance analysis of coded free-space optical links over Gamma-Gamma atmospheric turbulence channels," *IEEE Trans. Wireless Commun.*, vol. 5, pp. 1229-1233, Apr. 2006.

[7] J. Li, J. Q. Liu and D. P. Tayler, "Optical communication using subcarrier PSK intensity modulation through atmospheric turbulence channels," *IEEE Trans. Commun.*, vol. 55, pp. 1598-1606, Aug. 2007.

[8] S. G. Wilson, M. Brandt-Pearce, Q. Cao and J. H. Leveque, "Optical repetition MIMO transmission with multipulse PPM," *IEEE J. Select. Areas Commun.*, vol. 9, pp. 1901-1910, Sept. 2005.

[9] S. G. Wilson, M. Brandt-Pearce, Q. Cao and J. H. Leveque, "Free-space optical MIMO transmission with Q-ary PPM," *IEEE Trans. Commun.*, vol. 53, pp. 1402-1412, Aug. 2005.

[10] K. Kiasaleh, "Performance of APD-based, PPM free-space optical communication systems in atmospheric turbulence," *IEEE Trans. Commun.*, vol. 53, pp. 1455-1461, Sept. 2005.

[11] W. Huang, J. Takayanagi, T. Sakanaka and M. Nakagawa, "Atmopheric optical communication system using subcarrier PSK modulation," *IEICE Trans. Commun.*, vol. E76-B, pp. 1169-1177, Sept. 1993.

[12] W. Popoola, Z. Ghassemlooy, J. Allen, E. Leitgeb and S. Gao, "Free-space optical communication employing subcarrier modulation and spatial diversity in atmospheric turbulence channel," *IET Optoelectronics*, vol. 2, pp. 16-23, Feb. 2008.

[13] W. O. Popoola and Z. Ghassemlooy, "BPSK subcarrier intensity modulated free-space optical communications in atmospheric turbulence," *IEEE/OSA J. Lightwave Technol.*, vol. 27, pp. 967-973, Apr. 2009.

[14] H. Samimi and P. Azmi, "Subcarrier intensity modulated free-space optical communications in K-distributed turbulence channels," *IEEE/OSA J. Opt. Commun. Netw.*, vol. 2, pp. 625-632, Aug. 2010.

[15] W. O. Popoola, Z. Ghassemlooy, and E. Leitgeb, "Free-space optical communication using subcarrier modulation in gamma-gamma atmospheric turbulence," *9th International Conference on Transparent Optical Networks (ICTON '07)*, vol. 3, pp. 156-160, July 2007.

[16] A. Al-Habash, L. C. Andrews, and R. L. Phillips, "Mathematical model for the irradiance probability density function of a laser beam propagating through turbulent media," *Opt. Eng.*, vol. 40, pp. 1554-1562, Aug. 2001.

[17] J. D. D. S. Lopez, A. A. Mondragon, F. J. Mendieta, and I. N. Hipolito, (2011), *Trends of the Optical Wireless Communications*, [Online], Available: http://www.intechopen.com/books/advanced-trends-in-wireless-communications/trends-of-the-optical-wireless-communications

[18] L. C. Andrews, R. L. Phillips, C. Y. Hopen and M. A. Al-Habash, "Theory of optical scintillation," *Journal of the Optical Society of America A*, vol. 16, pp. 1417-1429, June. 1999.

[19] S. Karp, R. M. Gagliardi, S. E. Moran, L. B. Stotts, *Optical Channel: Fibers, Clouds, Water and the Atmosphere*, Plenum Press, 1988.

[20] E. J. Lee and V. W. S. Chan, "Part 1: Optical communication over the clear turbulent atmospheric channel using diversity," *IEEE J. Select. Areas Commun.*, vol. 22, pp. 1896-1906, Nov. 2004.

[21] X. Zhu, J. M. Kahn and J. Wang, "Mitigation of turbulence-induced scintilation noise in free-space optical links using temporal-domain detection techniques," *IEEE Photonics Technology Letters*, vol. 15, pp. 623-625, Apr. 2003.

[22] J. H. Churnside and R. G. Frehlich, "Experimental evaluation of lognormally modulated Rician and IK models of optical scintillation in the atmosphere," *J. Opt. Soc. Am.*, vol. 6, pp. 1760-1766, Nov. 1989.

[23] T. Lueftner, C. Kroepl, M. Huemer, J. Hausner, R. Hagelauer and R. Weigel, "Edge-position modulation for high-speed wireless infrared communications," *IEE Proc. Opto-electron.*, vol. 150, pp. 427-437, Oct. 2003.

[24] X. Song and J. Cheng, "Optical communication using subcarrier intensity modulation in strong atmospheric turbulence," *IEEE/OSA J. of Lightwave Technol.*, vol. 30, pp. 3484-3493, Nov. 2012.

[25] G. P. Agrawal, "*Fiber-Optical Communication Systems*," 2nd ed. New York: Wiley, Aug. 1997.

[26] R. L. Phillips and L. C. Andrews, "Measured statistics of laser-light scattering in atmospheric turbulence," *J. Opt. Soc. Am.*, vol. 71, pp. 1440-1445, Dec. 1981.

[27] J. C. Brandenburg and J. Q. Liu, "Signal detection in optical communications through the atmospheric turbulence channel," *Proc. IEEE Global Telecommun. Conf.*, New Orleans, USA, 2008, pp. 2741-2745.

[28] Andrews, L. C., Phillips, R. L., and Hopen, C. Y., "Laser Beam Scintillation with Applications," *S*PIE Press, 2001

[29] N. Wang and J. Cheng, "Moment-based estimation for the shape parameters of the Gamma-Gamma atmospheric turbulence model," *Opt. Express*, vol. 18, pp.12824-12831, June 2010.

[30] E. Bayaki, R. Schober, and R. K. Mallik, "Performance analysis of MIMO free-space optical systems in Gamma-Gamma fading," *IEEE Trans. Commun.*, vol. 57, pp. 3415-3424, Nov. 2009.

[31] I. S. Gradshteyn and I. M. Ryzhik, *Table of Integrals, Series, and Products*, 7th ed. San Diego: Academic Press, 2007.

[32] E. Jakeman and P. Pusey, "Significance of K distributions in scattering experiments," *Phys. Rev. Lett.*, vol. 40, pp. 546-550, Feb. 1978.

[33] E. Jakeman, "On the statistics of K-distributed noise," *J. Phys. A: Math. Gen.*, vol. 13, pp. 31-48, 1980.

[34] K. Kiasaleh, "Performance of coherent DPSK free-space optical communication systems in K-distributed turbulence," *IEEE Transactions on Communications*, vol. 54, pp. 604-607, Apr. 2006.

[35] M. Niu, J. Cheng and J. F. Holzman, "Error rate analysis of M-ary coherent free-space optical communication systems with K-distributed turbulence," *IEEE Trans. Commun.*, vol. 59, pp. 664-668, Mar. 2011.

[36] E. Jakeman and P. N. Pusey, "A model for non-Rayleigh sea echo," *IEEE Trans. Antennas Propag.*, vol. 24, pp. 806-814, Nov. 1976.

[37] A. Belmonte and J. M. Kahn, "Capacity of coherent free-space optical links using atmospheric compensation techniques," *Opt. Express*, vol. 17, pp. 2763-2773, Feb. 2009.

[38] R. Eaves and A. Levesque, "Probability of block error for very slow Rayleigh fading in Gaussian noise," *IEEE Trans. Commun.*, vol. 25, pp. 368-374, Mar. 1977.

[39] B. Maranda and C. Leung, "Block error performance of noncoherent FSK modulation on Rayleigh fading channels," *IEEE Trans. Commun.*, vol. 32, pp. 206-209, Sept. 1984.

[40] P. Loskot and N. C. Beaulieu, "Prony and polynomial approximations for evaluation of the average probability of error over slow-fading channels," *IEEE Trans. Veh. Technol.*, vol. 58, pp. 1269-1280, Mar. 2009.

[41] M. Chiani, D. Dardari, and M. K. Simon, "New exponential bounds and approximations for the computation of error probability in fading channels," *IEEE Trans. Wireless Commun.*, vol. 2, pp. 840-845, July 2003.

[42] J. W. Craig, "A new, simple and exact result for calculating the probability of error for two-dimensional signal constellations," *IEEE MILCOM Conf. Rec.*, Boston, MA, Nov. 4-7, 1991, pp. 25.5.1-25.5.5.

[43] Z. Wang and G. Giannakis, "A simple and general parameterization quantifying performance in fading channels," *IEEE Trans. Commun.*, vol. 51, pp. 1389-1398, 2003.

[44] M. Abramowitz and I. A. Stegun, "Handbook of mathematical functions with formulas, graphs, and mathematical tables," US Department of Commerce, 1964.

[45] N. C. Beaulieu, "A simple series for personal computer computation of the error function $Q(\cdot)$," *IEEE Trans. Commun.*, vol. 37, pp. 989-991, Sept. 1989.

[46] P. O. Borjesson and C. E. Sundberg, "Simple approximation of the error function $Q(x)$ for communication applications, " *IEEE Trans. Commun.*, vol. 27, pp. 639-643, Mar. 1979.

[47] C. Tellambura, Y. Dhungana and M. Soysa, "Uniform approximations for wireless performance in fading, noise and interference, " *Proc. ICC*, Ottawa, Canada, June 10-15, 2012, pp. 2410-2415.

Appendices

Appendix A

Truncation Error Analysis

The truncation error caused by eliminating the infinite terms after the $L+1$ terms in (3.10) can be defined as

$$\varepsilon_L = \sum_{m=M+1}^{N} \sum_{k=0}^{N-m} \sum_{p=L+1}^{\infty} \binom{N}{m} \binom{N-m}{k} (-1)^k \left(\frac{1}{2}\right)^{m+k+1} \frac{1}{p!} \left(\frac{\alpha\beta}{\sqrt{\eta\bar{\gamma}(m+k)}}\right)^p \times \left[u_{p1}(\alpha,\beta) + u_{p1}(\beta,\alpha)\right] \tag{A.1}$$

where

$$u_{p1}(x,y) = \frac{\Gamma(x-y)\Gamma(1-x+y)}{\Gamma(x)\Gamma(y)\Gamma(p-x+y+1)} \left(\frac{xy}{\sqrt{\eta\bar{\gamma}(m+k)}}\right)^y. \tag{A.2}$$

Using the Taylor series expansion of exponential function, we can simplify the summation term in (A.1) to be

$$\sum_{p=L+1}^{\infty} \frac{1}{p!} \left(\frac{\alpha\beta}{\sqrt{\eta\bar{\gamma}(m+k)}}\right)^p = \exp\left(\frac{\alpha\beta}{\sqrt{\eta\bar{\gamma}(m+k)}}\right). \tag{A.3}$$

We then obtain an upper bound of the truncation error of BLER employing NCFSK in (3.10) as

$$\varepsilon_L \leq \sum_{m=M+1}^{N} \sum_{k=0}^{N-m} \binom{N}{m} \binom{N-m}{k} \left(\frac{1}{2}\right)^{m+k+1} \max_{p>L}[u_{p1}(\alpha,\beta) + u_{p1}(\beta,\alpha)] \exp\left(\frac{\alpha\beta}{\sqrt{\eta\bar{\gamma}(m+k)}}\right). \tag{A.4}$$

After examing the first term in (A.2), we find that $u_{p1}(\alpha,\beta)$ or $u_{p1}(\beta,\alpha)$ approaches zero as p tends to infinite. Therefore, the truncation error ε_L diminishes with increasing index p. Similarly, we can obtain an upper bound of the truncation error for BLER employing BPSK in (3.34) as

$$\begin{aligned}\varepsilon_L \leq & \sum_{m=M+1}^{N} \sum_{k=0}^{N-m} \sum_{t=0}^{m+k} \sum_{l=0}^{t} \binom{N}{m} \binom{N-m}{k} \binom{m+k}{t} \binom{t}{l} \frac{1}{2} \left(\frac{1}{24}\right)^{m+k-t} \left(\frac{5}{24}\right)^{t-l} \left(\frac{1}{6}\right)^{l} \\ & \times \max_{p>L} [u_{p2}(\alpha,\beta) + u_{p2}(\beta,\alpha)] \exp\left(\frac{\alpha\beta}{\sqrt{\bar{\gamma}(m+k+3t-\frac{29}{10}l)}}\right)\end{aligned} \tag{A.5}$$

where

$$u_{p2}(x,y) = \frac{\Gamma(x-y)\Gamma(1-x+y)}{\Gamma(x)\Gamma(y)\Gamma(p-x+y+1)} \left(\frac{xy}{\sqrt{\bar{\gamma}(m+k+3t-\frac{29}{10}l)}}\right)^{y}. \tag{A.6}$$

Appendix B

Asymptotic BLER Using Mellin Transform

An alternative method to obtain the block error rate of NCFSK/DPSK in high SNR regimes is to use the Mellin transform of the conditional BLER. Recall the PDF of the optical irradiance I is given by (2.23). Letting $Y = I^2$, the PDF of Y is

$$f_Y(y) = \frac{1}{2}\sum_{p=0}^{\infty}\left[a_p(\alpha,\beta)y^{\frac{p+\beta-2}{2}} + a_p(\beta,\alpha)y^{\frac{p+\alpha-2}{2}}\right]. \tag{B.1}$$

The instantaneous SNR is $\gamma = \bar{\gamma}Y$. The PDF $f_Y(y)$ near the origin (i.e., $y \to 0^+$) can be approximated by

$$f_Y(y) = ay^t + o(y^{t+\varepsilon}) \tag{B.2}$$

where $\varepsilon > 0$, and a is a positive constant. The parameter t represents the order of smoothness of $f_Y(y)$ at the origin, and both a and t can be determined by the PDF $f_Y(y)$.

Assuming $\beta < \alpha$, as $y \to 0^+$, we can neglect the second term of (B.1) and approximate $f_Y(y)$ as

$$f_Y(y) \approx \frac{1}{2}a_0(\alpha,\beta)y^{\frac{\beta-2}{2}}. \tag{B.3}$$

Comparing (B.3) with (B.2), we obtain $a = \frac{1}{2}a_0(\alpha,\beta)$ and $t = \frac{\beta-2}{2}$.

The Mellin transform of the conditional block error rate in (2.36) can be written as

$$H(s) = \sum_{m=M+1}^{N} \sum_{k=0}^{N-m} \binom{N}{m} \binom{N-m}{k} (-1)^k \left(\frac{1}{2}\right)^{m+k} \int_0^\infty x^{s-1} e^{-x\eta(m+k)} dx \tag{B.4}$$

where $H(s)$ is the Mellin transform of $h(x)$, and $h(x)$ is the conditional probability of block error given by

$$h(x) = \sum_{m=M+1}^{N} \binom{N}{m} \left(\frac{1}{2}e^{-\eta x}\right)^m \left(1 - \frac{1}{2}e^{-\eta x}\right)^{N-m}. \tag{B.5}$$

Using [31, eq. 3.381(4)], we can simplify (B.4) as

$$H(s) = \sum_{m=M+1}^{N} \sum_{k=0}^{N-m} \binom{N}{m} \binom{N-m}{k} (-1)^k \left(\frac{1}{2}\right)^{m+k} \left[\frac{1}{\eta(m+k)}\right]^s \Gamma(s). \tag{B.6}$$

According to Proposition 1 described in [47], the asymptotic block error rate in high SNR regimes can be approximated by

$$P_{GG,asym}^{nc} \approx \frac{aH(t+1)}{\bar{\gamma}^{t+1}} = \frac{1}{2} a_0(\alpha,\beta) \frac{H(\frac{\beta}{2})}{\bar{\gamma}^{\frac{\beta}{2}}}. \tag{B.7}$$

Substituting (B.6) into (B.7), we can also obtain (3.37).